Ultrasonics Sonochemistry 120 (2025) 107465

Contents lists available at ScienceDirect

Ultrasonics Sonochemistry

journal homepage: www.elsevier.com/locate/ultson

Sonication-assisted *nonpolar-antisolvent* approach to produce cellulose suspensions, disaggregated by a *nonpolar-antisolvent* with orthogonal Kamlet-Taft acidity/basicity: Roles of *net-basicity* and *cosolvency*

Sergio E. Domínguez [a,*], Alexander S. Novikov [b,c,**], Dmitry A. Kornilov [d], Antti Vuolle [a], Mia Meriläinen [a], Hiram Isaac Beltrán [e]

[a] Department of Chemistry, Turku University Centre for Materials and Surfaces (MatSurf), Vatselankatu 2, FI-20014 Turku, Finland
[b] Institute of Chemistry, Saint Petersburg State University, Universitetskaya Nab. 7/9, 199034 Saint Petersburg, Russian Federation
[c] Research Institute of Chemistry, Peoples' Friendship University of Russia (RUDN University), Miklukho-Maklaya Str. 6, 117198 Moscow, Russian Federation
[d] Institute of Chemistry and Protection in Emergency Situations, Ufa University of Science and Technology, Zaki Validi 32, Republic of Bashkortostan 450076, Ufa, Russian Federation
[e] Department of Engineering and Basic Sciences, Metropolitan Autonomous University Campus Azcapotzalco (UAM-A), Av. San Pablo 420. Col. Nueva El Rosario Alcaldía Azcapotzalco C.P. 02128, Mexico City, Mexico

ARTICLE INFO

Keywords:
Sonication
Amorphous cellulose
antisolvent (AKA anti-solvent, nonsolvent, non-solvent)
Hydrogen-bond
Kamlet-Taft
Net-basicity
Disaggregation/deagglomeration

ABSTRACT

This work reports a simple sonication-assisted approach to produce diluted (0.5 mg/mL) suspensions of cellulose in the non-functionalizing nonpolar-antisolvent tetrahydrofuran (THF), which has a purely basic character (null Kamlet-Taft acidity parameter, $\alpha = 0$), by using it as medium to sonicate microcrystalline cellulose (MCC) at 40 kHz/70 Watts. The suspensions are obtained because of the high reactivity of the amorphous regions within MCC and its capability to behave as a (Turbak) acid, together with the low viscosity and surface tension of THF, and most importantly because of the positive *0.55* net-basicity of THF, comparable to that of ionic liquids (ILs) or deep eutectic solvents (DESs) used to dissolve cellulose in polar conditions. This was demonstrated by chloroform ($CHCl_3$), which cannot generate suspensions despite having similar values of viscosity, surface tension and molar volume than THF, however having a null basicity parameter, $\beta = 0$. (Complementary computational qualitative analyses using model molecules & conditions also show thermodynamic favorability of THF over $CHCl_3$). FTIR suggest a decrease of around 5 % in the crystallinity of cellulose after sonication in THF, while DLS show that adding $CHCl_3$ to the suspension in THF promotes disaggregation despite the THF-CHCl3 has a smaller net-basicity than THF, thus demonstrating cosolvency (instead of cononsolvency). (Complementary Langmuir trough experiments at the surface of water also demonstrate disaggregation because of $CHCl_3$ instead of moisture).

Despite the THF-$CHCl_3$ pair has been used previously to analyze the supramolecular properties of different polymers, this work uses it to analyze disaggregation in two antisolvents. This approach could constitute a platform to perform studies of dissolution/regeneration under null polarity, using proper probes (*e.g.* ILs or DESs), substrates and matrices.

1. Introduction

Cellulose is constituted by chains of several hundreds to tens of thousands of β(1,4)-D-glucopyranose units arranged in a linear structure, where every next glucose residue is rotated 180° along the 1,4 positions *via* glycosidic linkages. [69] Such an arrangement, together with a high degree of inter-chain packing generates an extensive network of intra- and inter-molecular hydrogen bonds (H-bonds) between the –OH hydroxyl groups at C2, C3, and C6 of the monomers, [14] and also van der Waals (vdW) interactions.(Paulsen [106]The H-bonding and vdW networks, together with the stiffness of the glycosidic linkage, generate crystalline domains having 2–20 nm in width and

* Corresponding author at: Department of Chemistry, Turku University Centre for Materials and Surfaces (MatSurf), Vatselankatu 2, FI-20014 Turku, Finland.
** Corresponding author at: Institute of Chemistry, Saint Petersburg State University, Universitetskaya Nab. 7/9, 199034, Saint Petersburg, Russian Federation.
E-mail addresses: sergioedominguez@gmail.com (S.E. Domínguez), a.s.novikov@spbu.ru (A.S. Novikov).

https://doi.org/10.1016/j.ultsonch.2025.107465
Received 31 October 2024; Received in revised form 11 May 2025; Accepted 1 June 2025
Available online 24 July 2025

lengths up to microns.(Mariano, Kissi, and Dufresne 2014) Such a structure generates a melting point above the temperature of degradation, [14]and nulls its dissolution in water and most organic solvents, since it requires the disruption of the H-bonding and vdW networks.

In plants cellulose is packed into microfibrils with a diameter of 5–50 nm and several micrometers in length with highly ordered crystalline regions, and also disordered (amorphous) regions, [107,121] in varying proportions depending on the raw material. [124] The amorphous domains have a higher accessibility and reactivity to mild processes such as swelling, [15] and harsher processes such as oxidation. [41] or acid hydrolysis. [121] (Chhavi [135] Crystalline cellulose materials can be purified by removing or reducing the extent of amorphous regions, obtaining for example microcrystalline cellulose (MCC), [73], 27)[133,153] and also nanocellulose (NC) materials, such as cellulose nanocrystals (CNCs)(Chhavi [121,135] and celulose nanofibers (CNFs), [41,86,121,133] Because of the relevance of MCC, [73], 27)[133,153] NC (CNCs, CNFs)[86,133,153] and amorphous materials, [11,66,95,120,123,124]studying crystalline and amorphous materials are active fields of research.

Chemical dissolution of cellulose is achieved by using solvent systems such as (i) those consisting of an aprotic polar solvent in combination with an inorganic salt (*e.g.* organic solvents with N,N-dimethylacetamide/LiCl or ammonium salts); [54])[94] (ii) aqueous solutions of metal complexes; (iii) ILs constituted by different anions and cations; [54,69] (iv) deep eutectic solvents (DESs) constituted by H-bonding donors and acceptors; [24]and also (v) methods with *potential* industrial applications such as the carbonate and carbamate chemical dissolution/regeneration processes.(El Seoud, Bioni, and Dignani 2021) In particular for ILs, *cosolvents* have shown to improve dissolution. (Chandrabhan [134](El Seoud, Bioni, and Dignani 2021) (El Seoud, Omar A. et al. 2019)[51] (Lihua [150] (Philipp categorized cellulose solvents into derivatizing, non-derivatizing, aqueous and non-aqueous). [77](For further details about cellulose solvents please see the reviews by[77]and[54]). In these media, the –OH groups of cellulose may behave according to *four* main categories proposed by Turbak in 1980: [77] (i) an acid, or H-bonding donor (*i.e* Cel–O–**H**–), in basic solvents (*e.g.* KOH alkali, Triton); (ii) a base, or H-bonding acceptor (*i.e.* Cel–**O**–(H)–), in acidic solvents (*e.g.* H_2SO_4, trifluoroacetic acid) or aqueous solutions of metal salts [89] (iii) a ligand, in a complexing agent solvent (*e.g.* Cuam, Cadoxen); or (iv) a reactive compound, converted to a soluble transient derivative or intermediate (*e.g.* xanthate, trifluoroacetate). These categories however have been considered to become less relevant in organic solvents of *limited* polarity and/or ionizability, [89]and to the best of our knowledge there are no reports focused on observing these chemical roles of cellulose in non-aqueous, non-derivatizing, nonpolar-antisolvents..

Cellulose is indeed not dissolved down to a molecular level, but rather forms stable colloidal dispersions with aggregates of at least several hundred chains, [89] mainly because of the strong tendency of cellulose to form H-bonding networks, which are not totally disintegrated. [94] Thus, small variations in solvent parameters such as composition, temperature, pH, water content, etc., can turn an effective solvent into one not even capable of swelling cellulose. [89] This sensitivity constitutes the driving force behind the process of *regeneration*, implemented in well-known methods such as the viscose or lyocell processes.(El Seoud, Bioni, and Dignani 2021) [40].

Regeneration typically involves the use of antisolvents (also named in the literature *anti-solvents*, *nonsolvents* or *non-solvents*). Research focused on regeneration is as important as that focused on dissolution, because it is an indispensable step for cellulose processing and shaping of novel materials.(El Seoud, Omar A. et al. 2019) Besides cellulose materials, antisolvents are critical to promote precipitation of nanoparticles in the food industry (using polysaccharides, proteins, biopolymer derivatives and surfactants),(Caicedo [17] to fractionate polysaccharides by precipitation,(X. Hu and Goff 2018) to precipitate/stabilize nanoparticles of hydrophobic drugs, [129] or as key morphology-directing agents in the context of solution-processed organic solar cells (OSCs) (labelled *additives*, when used at concentrations < 10 % v/v, for cosolvents and antisolvents). [87].

Understanding the interaction forces controlling dissolution and regeneration of cellulose materials is an active field of research. El Seoud et al.(El Seoud, Omar A. et al. 2019) reviewed the advances on the understanding of the mechanisms of cellulose *dissolution and regeneration*, in ILs and alkaline solutions, focusing on parameters such as solution rheology and microscopic solvent/solution properties such as empirical polarity, Lewis acidity/basicity and dipolarity/polarizability, using experimental and computational approaches. On the same year Verma et al.(Chandrabhan [134] contributed with a review on the dissolution of cellulose in ILs *and cosolvents*, while later Shamsuri et al. [117] contributed with a review on the properties and applications of cellulose regenerated from ILs and cosolvents. Overall the regeneration mechanism follows steps that are similar to those occurring during the crystallization of the (native) cellulose I allomorph: (1) formation of mini-sheets by vdW forces, (2) association of these sheets in "mini-crystals" by H-bonding, and (3) convergence of the crystals into larger *crystalline or amorphous* arrangements, depending on factors such as the solution itself, degree of polymerization (DP), temperature and antisolvents.(El Seoud, Omar A. et al. 2019) By exchanging solvent and antisolvent, inter- and intra-molecular H-bonds are reestablished, resulting in the precipitation and regeneration of the dissipated cellulose chains. [10] The exchange between solvent and antisolvent molecules is considered the main driving force initiating the reformation of cellulose,(El Seoud, Omar A. et al. 2019)[10,79] with diffusive processes leading to the reformation of intra- and inter- H-bonds previously broken during dissolution. [79] In the case of solutions in eutectic solvents such as ILs (or DESs), tertiary systems are formed because of their constituting anions and cations (or H-bonding donor or acceptor). In such systems the use of different *polar* antisolvents (*e.g.* water, ethanol, methanol, acetone, acetonitrile, etc.) have shown to allow a fine tuning of the macroscopic morphology of the regenerated cellulose, depending on the interactions between the dissolved (amorphous) cellulose and the regeneration antisolvent, [10] (H. [139] with water having the most relevant role as antisolvent overall [79].

All of these investigations on dissolution/regeneration involve *adding antisolvents to solutions*, however using nonpolar antisolvents alone has not been studied to our knowledge. Analyzing aggregation/disaggregation using nonpolar-antisolvents alone, could offer a platform to study dissolution/regeneration under null (or low) polarity.

The acid-base concept, has been extensively used in connection with polysaccharides, as a more general and quantitative extension of the traditional H-bonding theory, which includes H-bonds possessing a wide range of strength values. [74] For example, Drago's method, used to analyze swelling in fibers indeed requires treating H-bonding interactions as an acid–base interaction. [15] In turn, swelling is an initial state of dissolution, because during its occurrence the cellulose pulp elements pass apart from each other while the solvent-filled void space grows. [155] In this regard the Gutmann donor number (DN) and acceptor number (AN), is a restatement of the generalized Lewis acid-base definition, which has been suggested to represent a fundamental way of understanding H-bonded systems such as fiber–fiber bonded systems, [74] that allows predicting (even quantitatively) the strength of Lewis acid-base interactions. [90] Similarly, the Kamlet-Taft scale can be used with an engineering approach in the field of lignocellulosic solvation, since it provides an useful framework for qualitative comparisons (*e.g.* see Table 1 in (Luyao [151]. From these two scales, Kamlet-Taft is considered to be a better measure of solvent/solute interactions, [90] since its parameters are determined by spectroscopic means *via* solvatochromic dyes in solution,(Lihua [42,43,52,130,150] while Gutmann parameters are determined using a calorimetric method. [90] Despite some authors have recently discussed on the appropriate choice of the Lewis-basicity parameters, in order to avoid an inadequate application to a presumed basicity effect, which can arise from an

Table 1
Values of γL, μ, dielectric constant (ε), molar volume (V), enthalpy of complexation with BF3 (for Lewis bases), and also Gutmann donor number (DN) and acceptor number (AN), Kamlet–Taft values (α, β, π*) and net-basicity and Hansen (δD, δP and δH) parameters of the solvents tested.(Sawyer D. T. and Roberts L. 1974) ("Viscosity, Surface Tension, Specific Density and Molecular Weight of Selected Liquids," n.d.)[147,49,12](Riddle and Fowkes 1990)[15,131,61,127,115](Liang, Xinquan et al. 2021)[4,70] (Luyao [151,7] The Kamlet-Taft parameters of ILs and DESs were measured at temperatures ranging in 70-100° C. (Luyao [151].

Type	*Solvent*	*γL (mN/m)*	*μ (cP)*	*Ref index*	*ε*	*V*	*Base enthalpy of complex.† (kJ/mol)*	*δD*	*δP*	*δH*
Non-polar	**$CHCl_3$**	26.7	0.54	1.44	4.81	80.7	–-	17.8	3.1	5.7
	THF	26.7	0.46	1.4	7.5	81.7	**90.4**	16.8	5.7	8.0
Polar-aprotic	**ACN**	28.7	0.37	–-	37.5	52.6	60.39	15.3	18	6.1
	DMSO	42.9	1.99	1.47	46.7	71.3	**105.34**	18.4	16.4	10.2
Polar-protic	**WATER**	72.7	0.89	–-	80	18	104.4	15.5	16	42.3

Type	*Solvent*	*DN (kcal/mol)*	*AN‡ (kcal/mol)*	*δ (DN-AN)*	*α*	*β*	*π**	*β − α*
Non-polar	**$CHCl_3$**	**0**	**5.4**	**−5.4**	**0.44**	**0**	**0.58**	**−0.44**
	THF	**20**	**0.5**	**19.5**	**0**	**0.55**	**0.58**	**0.55**
Polar-aprot.	**ACN**	14.1	4.7	9.4	0.2	0.4	0.7	0.2
	DMSO	29.8	3.1	**26.7**	0	0.76	1	0.76
Polar-prot.	**WATER**	18	15.1	2.9	1.2	0.5	1.2	−0.7
	ButAcid	–-	–-	–-	1.06	0.22	0.47	−0.84
	OctAcid	–-	–-	–-	0.94	0.23	0.38	−0.71
ILs	**[EtMeIm] AcO**	43.3	–-	–-	0.4	0.95	1.08	0.55
	[EtMeIm] PF6	−6.2	–-	–-	0.76	0.2	0.99	−0.54
	[BMeIm] AcO	–-	–-	–-	0.43	1.05	–-	0.62
	[BMPyr] DCN	–-	–-	–-	0.29	0.52	1.18	0.23
	[EtMeIm] FAP	−12.3	29.3	−41.6	0.58	0.11	1.04	−0.47
	[EtMeIm] DCN	37.8	31.7	6.1	0.53	0.63	1.11	0.1
DESs	**[N4444] Cl-OctAcid**	–-	–-	–-	0.84	1.19	0.8	0.35
	[N2222] Cl-OctAcid	–-	–-	–-	0.96	0.87	0.81	−0.09
	TBAC-EG (1:2)	–-	–-	–-	0.709	0.805	–-	0.096
	TBAC-LA	–-	–-	–-	0.614	0.617	1.083	0.003

† According to the the BF3 Affinity Scale ("The BF3 Affinity Scale" 2009).
‡ (Riddle and Fowkes 1990),[4].
Acronyms: ButAcid: butanoic acid; OctAcid: octanoic acid; [EtMeIm]PF6: 1-ethyl-3-methylimidazolium (cation) – hexafluorophosphate (anion); [EtMeIm]AcO: 1-ethyl-3-methylimidazolium (cation) – acetate (anion); [BMPyr]DCN:; [EtMeIm]FAP:; [EMIM]DCN:; [N4444]Cl-OctAcid: tetrabutylammonium chloride (H-bond acceptor)(HBA) – octanoic acid (H-bond donor)(HBD); [N2222]Cl-OctAcid: Tetraethylammonium chloride (HBA) – octanoic acid (HBD); TBAC-LA: tetrabutyl ammonium chloride (HBA) – lactic acid (HBD); ChCl-LA: choline chloride (HBA) – lactic acid (HBD).

interaction with either an isolated molecule (ligand) or with a medium (solvent effect), [45] Gutmann and Kamlet-Taft scales have been used to analyze the swelling [15,74] or dissolution of cellulosic materials. (Luyao [151].

This work presents a simple sonication-driven nonpolar-antisolvent approach to obtain suspensions of cellulose in the non-functionalizing, nonpolar, purely basic (null value of Kamlet-Taft acidity, or H-bonding donating ability) antisolvent tetrahydrofuran (THF), by applying sonication (with frequency and power of 40 kHz and 70 Watts respectively) to its mixture with microcrystalline cellulose (MCC) during 15 to 90 min at room temperature, and subsequently filtering *the supernatant* through a filter membrane (with 450 nm cutoff). (Sonication is widely used in the field of cellulosic materials, while filtering is analogous to fractionation methods such as field-flow fractionation (FFF), gravitational sedimentation and centrifugal fractionation, see the Materials section for details). Gravimetry and Fourier transform infrared spectroscopy (FTIR) were used to quantify and verify (respectively) the presence of cellulose in the residual solvent after sonication and filtration in different solvents. Complementary density functional theory (DFT) and non-covalent interactions analysis (NCI) computational simulations were used to analyze qualitatively the thermodynamic favourability of association of cellulose with THF, $CHCl_3$, and other relevant solvents, following recent literature on cellulose materials (see the Materials section). Dynamic light scattering (DLS) was used to study the concentration-driven aggregation of the suspended particles in THF, and also to analyze the disaggregation caused by the addition of $CHCl_3$ as a second nonpolar-antisolvent with orthogonal Lewis acidity/basicity (null value of Kamlet-Taft basicity, or H-bonding accepting ability).

To the best our knowledge, in the literature there are not previous reports with the *scope of the present work: analyzing disaggregation of cellulose particles in purely nonpolar media constituted by two antisolvents, using the Kamlet-Taft solvent scale to rationalize the experimental results.*

2. Materials and methods

In this work it was used commercial high-purity microcrystalline cellulose (MCC) from cotton linters for partition-chromatography (Sigma-Aldrich, product no. 310697), with 20 μm crystalline microfibrils, crystallinity index CI ≈ 1.05 or 0.63 (by FTIR or XRD), degree of polymerization (DP) ≈ 251, [85] molar mass Mn ≈ 61,700 g/mol, [80] and dispersity Đ = Mw/Mn ≈ 5.("Cellulose microcrystalline, powder, 20um 9004–34-6," n.d.) (Notice that in literature there is a lack of consensus in regard to DP, with reports of values ranging in 40–200). (Kalász, Báthori, and Valkó 2020, 10).

2.1. Antisolvents selection and Lewis acidity/basicity orthogonality

Four organic solvents incapable of dissolving cellulose (*i.e.* cellulose antisolvents) from Sigma-Aldrich were used as received, polar-aprotic dimethylsulfoxide (DMSO) and acetonitrile (ACN), and nonpolar [103] tetrahydrofuran (THF) and chloroform ($CHCl_3$). (For the DLS experiments it was used THF stored in a glovebox under Nitrogen atmosphere). Table 1 shows values of some relevant parameters of these solvents, while Table 1 *cont.* also shows the values of Gutmann and Kamlet-Taft acidity/basicity parameters, including the net-basicity, defined as the difference between the DN and AN for the Gutmann scale, [15,126] and the "β – α" difference for the Kamlet-Taft scale. (Luyao [151] For comparison purposes, these tables also show water and some polar (protic and aprotic) organic solvents, [127] together with some ILs [115 4] and DESs. [127](Liang, Xinquan et al. 2021).

We used antisolvents with an useful range of viscosity (μ) and surface tension (γL) values, which are the main physical–chemical parameters

impacting on the quality of cavitation during sonication. [5] (Viscosity is also known to exert a significant effect on self-assembly processes). [28] These antisolvents also provide an useful range of values in regard to Lewis acid-base properties. The null Kamlet-Taft H-Bonding accepting ability of $CHCl_3$ ($\beta = 0$), is completely opposite to the null H-bonding donating ability of THF ($\alpha = 0$). Thus it seems reasonable defining THF and $CHCl_3$ as *orthogonal* in regard to their Lewis acidity/basicity (for further details on this label please see Section S-1. in the Supplementary File). To our knowledge, this aspect has not been highlighted in the literature, despite previous works with different polymers such as hexanoyl-chitosan, [109] polyphenylacetylene (PPA) [19] or poly (methyl methacrylate) (PMMA) (a linear unbranched homopolymer, similarly to cellulose), [12,13]have shown that the $CHCl_3$-THF pair is useful to analyze the aggregation of polymeric molecules.

Beyond using THF stored in a glovebox, moisture was not controlled during the experimental procedures. For details on the validity of invoking the Kamlet-Taft parameters under such conditions please see Section S-1.1. in the Supplementary File, and also the results obtained onto the surface of water using the Langmuir trough instrument, detailed ahead.

2.2. Sonication

In the present work, for each antisolvent tested, glass-sealed flasks with 5 mL of mixtures at 20 mg of MCC per mL of antisolvent were sonicated during 15, 40, 60 or 90 min, using a Bransonic 1510R-DTH, 1.89 L water-bath, ultrasonicator (Branson Ultrasonics Co.) operating at a frequency of 40 kHz and power of 70 W, at room temperature (25 °C), always placing the samples at the same place (at the middle-center) an depth in the sonicator water bath. (For further details on the working principle of sonication and its use in the context of cellulose, see Section S-2 in the Supp. File).

2.3. Filtration as fractionation method

Filtration was used as a simple *fractionation* method, which allows homogenizing a particular desired particle size of the cellulose present in the solvent. For further details and references within the context of the present work please see Section S-3 in the Supplementary File.

In the present work, the supernatant of the sonicated samples was micro-filtered through a polytetrafluoroethylene filter membrane with a pore size cutoff of 450 nm (HPLC syringe filter, Grace Davison Discovery Science), previously used by Hu and Abidi,(Y. [57] Brinkmann [16] and Jakubek et al. [62]to filter CNCs,

2.4. Gravimetry

Gravimetry was used by quintuplicate as a simple method *to estimate the mass* of cellulose possibly present in each antisolvent after sonication (its presence was *verified* using FTIR spectroscopy). Gravimetry was implemented by weighing (i) the dried remaining of MCC powder, and (ii) all the materials that had contact with the polymer (*i.e.,* PTFE filter membrane, syringe, and glassware) prior and after filtration, and then performing a mass balance. Samples of 5 mL showed to be adequate in generating standard deviation values of around ± 10 % of the average estimations.

2.5. Fourier transform infrared (FTIR) spectroscopy

A Bruker Tensor 27 IR spectrometer was used to analyze the different cellulose samples by in the 3800–800 cm^{-1} wavelength range, analyzing THF alone (*versus* air as blank), un-sonicated MCC powder (*versus* a dried KBr crystal as blank), 0.5 mg/mL cellulose-THF suspensions obtained after 15 min of sonication (*versus* THF as blank), and a cellulose drop-casted film using such suspension (*versus* the underlying silicon (Si/SiO_2) surface as blank). The cellulose films were obtained by drop-casting the THF suspensions (obtained after 15 min of sonication) onto Si/SiO_2 wafers and gently removing excess material with aid of a stream of compressed N_2, and repeating the process until observing a film with the naked eye. The Si/SiO_2 substrates were previously washed in piranha solution (sulphuric acid and hydrogen peroxide combine with the formation of peroxymonosulfuric acid), which is a well-known cleaning method of Si/SiO_2 wafers in the semiconductor industry to promote silane attachment, since it is capable of removing contaminants and promoting hydroxylation,(O'Mahony Tom F. and Morris Michael A. 2021) (*i.e.* increase the *silanol number*). [154].

FTIR data was also used to estimate *qualitatively* the change in crystallinity due to the sonication treatment in THF, using the Nelson & O'Connor indexes: Cr.R1 = A_{1372}/A_{2900} and Cr.R2 = A_{1430}/A_{893} (where A stands for the absorbance value at the wavenumbers indicated in subscripts). [113] Estimation of the crystallinity index (CI) with FTIR is the simplest method available (when compared with XRD and/or NMR), [104 113] and despite giving only *relative* values (because the spectrum always contains contributions from both crystalline and amorphous regions), [104] it provides reliable estimations of the CI. [85].

2.6. Dynamic light scattering (DLS)

DLS was used to estimate (i) the apparent hydrodynamic radius (R_h) distribution, and (ii) the decay time of the correlation function generated by suspensions either in pure THF (labelled $X_{CHCl3} = 0$) with concentrations of 0.5, 0.25 and 0.1 mg/mL, or in THF-$CHCl_3$ mixtures with compositions of 80 and 90 % (v/v) of $CHCl_3$ (labelled $X_{CHCl3} = 0.8$ & 0.9) at 0.1 mg/mL. The addition of $CHCl_3$ was used to analyze the tuning disaggregation via a second nonpolar-antisolvent with opposite Lewis acid-base properties. DLS has been used previously to perform qualitative comparisons of the Rh values in different organic solvents, analyzing the dispersibility of NCC, [137] or aggregates of polythiophene-fullerene pairs.(Domínguez, Kohn, et al. 2021).

The measurements were performed under the same conditions reported by the author previously, (Domínguez, Kohn, et al. 2021)[31]at 25 °C using a Zetasizer Nano-ZS (Malvern Instruments Ltd, England). In order to minimize dust interference, (i) the scattered light was collected at 173°, *i.e.* using non-invasive backscatter detection, which increases sensitivity;(Montes A., Pereyra C., and Martinez de la Ossa E. J. 2015) ("Dynamic Light Scattering: An Introduction in 30 Minutes" 2014)) [64,142,108,27] (ii) the cuvette was cleaned using ethanol and a direct flow of compressed air before each measurement; and (iii) all samples were filtered with 5 − 6 μm poly(tetrafluoroethylene) syringe filter membranes, avoiding the sample to slip through the internal walls of the cuvette.

In order to obtain highly reliable DLS measurements it is required non-absorption of light by the particles, reduced multiple scattering, dilute solutions, and exact values of viscosity and refractive index of the solutions. [71]In the present work the particles under study are not photoactive, the suspensions are diluted, and the values of viscosity and refractive index of THF and THF-$CHCl_3$ mixtures with 80 and 90 % of $CHCl_3$ (v/v) have been reported in the literature to be 0.575 and 0.557 cP for the viscosity,(Sólimo and Gomez Marigliano 1993) and 1.415 and 1.41 for the refractive index, [44] respectively.

The values of the correlation coefficient and decay times were also analyzed since size-monodisperse samples generate steeper decays. ("Dynamic Light Scattering: An Introduction in 30 Minutes" 2014)) [64,142,108,27].

For details on the theoretical background of the DLS technique and also on the use of this technique within the context of cellulosic materials please see Section S-4 in the Supplementary File.

2.7. Langmuir trough instrument

In order to form and compare films of underivatized cellulose at the air/water interface (Langmuir films) using X_{CHCl3} = 0, 0.8 & 0.9

suspensions, it was used a KSV Langmuir minitrough with 100 cm^2 of surface area and 40 mL of sub-phase volume, with two computer-controlled motorized movable barriers and a platinum rod sensor tensiometer (resolution of 0.01 mN/m). THF has been used previously as spreading solvent to form Langmuir films of molecules such as C_{60} fullerene [97] or iron phthalocyanine, [112]while $CHCl_3$ is commonly used in such kind of experiments. [83] The Langmuir films were generated by spreading a defined volume of different cellulose suspensions onto the clean air/water interface using a mycro-syringe, to obtain a surface concentration of 0.25 mg/m^2 for the $X_{CHCl3} = 0$ & 0.8 films, and 0.125 mg/m^2 for the $X_{CHCl3} = 0.9$ films, dividing the total dropped volume in at least 3 drops at different points of the surface of water, from a position as close as possible to to the surface of water, and then waiting 15 min for solvent evaporation. This is a commonly used time period to allow evaporation, [67] regardless, the evaporation was verified experimentally by a constant surface pressure reading. Scheme S-1 in the Supplementary File shows a visual explanation of the procedures performed at the Langmuir trough instrument; *In detail*: Surface pressure-molecular area isotherms were obtained by recording the surface pressure generated by the films when changing the position of the movable barriers in the instrument at 15 mm/min. The area occupied by the aggregates at the air/water interface is estimated by extrapolating the slope of the Π-A isotherm to zero surface pressure.

2.8. Atomic force microscopy (AFM) to drop-casted films

In the present work AFM micrographs of drop-casted films onto Si/SiO_2 substrates were used to confirm or discard the presence of structured materials such as CNCs or CNFs in the solvent after sonication. The measurements were performed under the same conditions reported by the author previously, [34](Domínguez, Vuolle, et al. 2021) inside of a class 100 clean room, under ambient conditions, in tapping mode, using silicon cantilevers (≈225 nm length, ≈20 nm tip-height, resonance frequency ≈84 kHz).

For detailed information and references about using AFM within the context of cellulosic extracted materials please see Section S-5 in the Supplementary File.

2.9. Computational complementary studies

In order to further rationalize the gravimetry results, complementary computational tools were used to obtain qualitative thermodynamic information of the interaction between single molecules of THF or $CHCl_3$ with a model molecule of cellulose (the cellobiose dimer) in a particular model conformation (*anti-syn*), also evaluating interactions with molecules of other solvents such as polar water, methanol and the acetate anion (AcO-). Cellobiose was selected as a model for cellulose since it contains β-D-pyranose units connected by the 1 −> 4 glycosidic bonds, which is defined by the presence of the oxygen atom connecting two pyranose units, thus making it capable of representing 1,4-β-glycosidic interactions together with inter- and intra-molecular H-bonding in cellulose.

On the other hand, the anti-syn conformation was selected because is the global minimum conformation of cellobiose in the gas phase, and has been extensively studied. [92]In regard to the solvents selected for the simulations, there were selected antisolvents, including obviously THF and $CHCl_3$.

The starting geometry of the cellobiose in the anti-syn conformation was extracted from the pre-optimized geometry provided by Mittal et al. after using the M06-2X level of theory. [92] The complexes between cellobiose and solvents or anions was carried by using the optimized structures provided by Mittal et al., substituting the solvent molecule. Then a full geometry optimization procedure for all model complexes was carried out at the DFT level of theory using the dispersion-corrected hybrid functional ωB97XD[22] with the help of Gaussian-09 ("Gaussian 09, Revision A.1, Gaussian, Inc. Gaussian 09, Revision A.02, M. J. Frisch, G. W. Trucks, H. B. Schlegel, G. E. Scuseria, M. A. Robb, J. R. Cheeseman, G. Scalmani, V. Barone, G. A. Petersson, H. Nakatsuji, X. Li, M. Caricato, A. Marenich, J. Bloino, B. G. Janesko, R. Gomperts, B. Mennucci, H. P. Hratchian, J. V. Ortiz, A. F. Izmaylov, J. L. Sonnenberg, D. Williams-Young, F. Ding, F. Lipparini, F. Egidi, J. Goings, B. Peng, A. Petrone, T. Henderson, D. Ranasinghe, V. G. Zakrzewski, J. Gao, N. Rega, G. Zheng, W. Liang, M. Hada, M. Ehara, K. Toyota, R. Fukuda, J. Hasegawa, M. Ishida, T. Nakajima, Y. Honda, O. Kitao, H. Nakai, T. Vreven, K. Throssell, J. A. Montgomery, Jr., J. E. Peralta, F. Ogliaro, M. Bearpark, J. J. Heyd, E. Brothers, K. N. Kudin, V. N. Staroverov, T. Keith, R. Kobayashi, J. Normand, K. Raghavachari, A. Rendell, J. C. Burant, S. S. Iyengar, J. Tomasi, M. Cossi, J. M. Millam, M. Klene, C. Adamo, R. Cammi, J. W. Ochterski, R. L. Martin, K. Morokuma, O. Farkas, J. B. Foresman, and D. J. Fox, Gaussian, Inc., Wallingford CT, 2016." 2009) program package. The standard 6-31G* basis sets were used for all atoms, in vacuum.

No symmetry restrictions were applied during the geometry optimization procedure. The Hessian matrices were calculated analytically for all optimized model structures to prove the location of the correct minima on the potential energy surfaces (no imaginary frequencies were found in all cases) and to estimate the thermodynamic parameters, the latter being calculated at 298.150 K and 1 atm.

The optimized geometries and cellobiose-solvent complexes were visualized with the Avogadro[50] and Jmol ("Jmol: An Open-Source Java Viewer for Chemical Structures in 3D. Http://Www.Jmol.Org/," n.d.) freeware packages. The Cartesian atomic coordinates for all model structures are provided in Tables S-3 to S-7 in the Supplementary File.

From the output files were performed analyses on (i) geometrical lengths of the structure of the anti-syn cellobiose in absence and presence of the solvent molecules; (ii) formation of inter-molecular H-bonds between the cellobiose and the solvent anions; (iii) interaction energies for all cellobiose-solvent complexes; (iv) thermodynamic free energy of the complexes and (v) noncovalent interactions analysis (NCI). The latter was performed by using the Multiwfn program (version 3.7),(T. [81]and results were visualized by using the VMD program.[59].

For further details on the solvent and antisolvent molecules used in the simulations, and references of the use of computational methods to simulate cellulose-solvent interactions, and the solvents selected in the simulations reported here, please see Section S-6 in the Supplementary File. On the other hand, for further details on the use of the ωB-97XD instead of M06 levels of chemistry please see Section S-6.1 in the supplementary file.

3. Results and discussion

3.1. Gravimetry

According to gravimetry, after sonication of MCC in THF and filtration, it is obtained a concentration of 0.5 mg/mL of cellulose, regardless of the sonication time. Despite being low, this concentration is useful under the scope of the present investigation (*analyzing disaggregation of cellulose particles in nonpolar media constituted by two antisolvents*). Besides THF, none of the other organic solvents tested (ACN, DMSO, $CHCl_3$) showed presence of cellulose by gravimetric means, after the sonication-assisted nonpolar-antisolvent procedure (this was verified with FTIR spectroscopy).

The fact that similar results are obtained from all of the sonication times evaluated (15, 40, 60 or 90 min), despite that after 60 min of sonication it is observed a modest increase in temperature in the sonicator water-bath (from 25 to approximately 37° C), suggests that 15 min of sonication are enough to remove as much reactive material as possible from the MCC using 40 kHz/70 Watts sonication in THF.

The filtered samples are fully transparent, without visible sedimentation, even after during 10 weeks (no longer periods were evaluated), which suggests the presence of particles within the colloidal range (1–1000 nm) (this was verified with DLS). Our results indicate that the

sonication-assisted nonpolar-antisolvent method reported here crosses the minimal physical–chemical energy threshold required to remove material from the MCC into the THF.

Because of (i) the high accessibility and reactivity of amorphous cellulose of different cellulose materials to mild and harsh physical–chemical processes discussed in the introduction; [15,41,121] (Chhavi [135,36,3,107](Nascimento et al. 2015) [26,102,133,107,101,86,137]and also (ii) that degradation of crystalline regions require high temperatures such as 80 °C; [3]) and also (iii) that THF has a nonpolar-antisolvent nature, [54,77] incapable of even *dispersing* suspensions of CNCs, [99]; it would be reasonable assuming that in THF the cellulose is present in the form of a suspension of mainly amorphous material. However, interestingly the FTIR data indeed suggests that the suspensions are constituted by cellulose less crystalline than the MCC starting material, however not purely amorphous (details ahead); On the other hand, DLS confirmed the suspension nature of the samples (details ahead).

Table 1 shows that among the antisolvents tested, THF and $CHCl_3$ have identical values of surface tension −cohesive forces- (γL), of 26.7 mN/m, which in turn are the lowest values of surface tension among all of the antisolvents. However, THF has a lower viscosity (μ) than $CHCl_3$, which indeed explains why the suspensions were obtained in THF but not in $CHCl_3$, since literature reports that solvents with small values of *both* surface tension and viscosity generate improved acoustic cavitation during sonication. [5]Regardless this reasoning provides alone a plausible explanation to our results, analyzing other molecular aspects of all the antisolvents provide a deeper insight on the system.

In regard to polarity, THF and $CHCl_3$ have the smallest values of dielectric constant (ε) and polar-Hansen solvent parameter (δP), with THF having a larger values than $CHCl_3$ by 56 and 83 % respectively. In this regard, the literature focused on acid-base interactions of cellulose, reports that factors such as dielectric constant [74] or dipole moment [15] show *weak* correlations with solubility. The same has been reported for studies focused on the aggregation of poly(methyl methacrylate) (PMMA), (a linear unbranched homopolymer, similarly to cellulose) which have not shown an obvious relationship between the solvent polarity and the ability to induce molecular changes on the polymer. [12].

In regard to the Hansen scale Table 1 shows that THF and $CHCl_3$ have similar values of the polar (δP) and H-bonding (δD), however $CHCl_3$ is not capable of causing cellulose to behave as a base. Finally, in regard to dispersive interactions, Tables 1 and 1 cont. show that all of the solvents tested have similar values of the dispersion-bonding Hansen (δD) and Kamlet-Taft π* parameters, which for the latter, is indeed the same for THF and $CHCl_3$.

3.2. The role of net-basicity during the sonication in antisolvents

Besides surface tension and viscosity, for cellulose materials is known that basicity (H-bonding accepting ability, DN, β) is the most important parameter related to cellulose-solvent interactions, followed by the Lewis acidity (H-bonding donating ability, AN, α) and the molar volume (V), [74,15] which defines the coefficients of swelling and diffusion. [15] (In regard to V, as Table 1 shows, THF and $CHCl_3$ have very similar values (81.7 and 80.7 respectively), which in turn are the largest values from all the solvents tested).

In regard to basicity, some studies have suggested that values of $\beta > 0.8$ are required for cellulose dissolution to take place. [1]Since in the present work the cellulose suspensions were obtained in THF (which has a Kamlet-Taft basicity of $\beta = 0.55$ and a null acidity $\alpha = 0$), but not in $CHCl_3$, (which has a null basicity $\beta = 0$ and an acidity of $\alpha = 0.44$) it is reasonable to propose that our results show that under the conditions tested, cellulose is capable of interact with the nonpolar-antisolvent THF acting as an acid, however it cannot interact with $CHCl_3$ by acting as a base, according to the categories proposed by Turbak in polar media. [77] As mentioned in the introduction, these categories have been considered to be less relevant in organic solvents of *limited* polarity and/or ionizability. [89] Thus, our results provide evidence of cellulose playing the role of an acid in a nonpolar environment, after applying supplementary physical energy (sonication, in the present work). As discussed by Gal and Maria, [45] a solute may be interact very weakly with the medium (to the point of being almost in a gas-phase situation), or may interact more strongly with the medium, in particular when Lewis acid-base forces enter into action. To our knowledge such an example was not discussed in the literature before.

Beyond basicity, in the context of catalysis, the interactions of solvents and catalysts are better described in terms of the *net-basicity*, defined as the difference between basicity and acidity: DN-AN in the scale of Gutmann, [52] or β–α for the Kamlet-Taft scale.(Luyao [151] For example, during the hydrogenation of benzyl alcohol, solvents with a *negative* net-basicity (methanol, ethanol and acetic acid), have shown to be analogous to *nonpolar* solvents (acetone, 1,4-dioxane, THF, and diethyl ether), while solvents with positive net-basicity (**THF,** ACN, 1,4-dioxane and diethyl ether), inhibited the reaction. [126]In this regard, after its null value of H-bonding acidity ($\alpha = 0$), THF possess a net-basicity of $\alpha\text{-}\beta = 0.55$, which as shown in Table 1 *cont.*, is indeed similar to some ILs such as 1-ethyl-3-methylimidazolium acetate ([EtMeIm]AcO) ($\alpha\text{-}\beta = 0.55$), and DESs such as or tetrabutylammonium chloride octanoic acid ([N444]Cl-OctAcid) ($\alpha\text{-}\beta = 0.35$), which are among the highest net-basicity values for these type of solvents. (Some other references estimate slightly different values of $\alpha = 0.41$ $\beta = 1.03$ and $\pi^* = 1.08$, with a net-basicity $\alpha\text{-}\beta = 0.62$ for [EtMeIm]AcO). [70] This is relevant because some of the highest cellulose solubility values correlate with large values of β and net-basicity from these ILs and DESs, as shown in Fig. 7 of (Luyao [151]. In this regard, despite DMSO is similar to THF in regard of also having a null value of α, and a high net-basicity $\alpha\text{-}\beta = 0.76$, it is not capable of generating suspensions of cellulose *via* sonication because of its large cohesive forces and viscosity, with the latter being 4 times larger than that of THF (see Table 1).

In resume, it seems reasonable to suggest that low values of surface tension and viscosity (which improve cavitation) and large values of molar volume are not capable alone to generate suspensions in a nonpolar-antisolvent *via* 40 kHz/70 Watts sonication, according to the results obtained with $CHCl_3$. Instead our results indicate the requirement of a positive, relatively large, positive *net-basicity* value, which is in agreement with the literature which indicates that acidity/basicity, and particularly the latter, is the most relevant parameter for cellulose dissolution. Our results also show that when using nonpolar-antisolvents the role of net-basicity remains dominating, such as in the cases of the euctectic ILs and DESs, for which is known that their basic component is the one leading the dissolution process of cellulose. To our knowledge, this work is the first highlighting the role of a high positive net-basicity (comparable to that in ILs and DESs) on the obtention of suspensions on underivatized cellulose in a nonpolar-antisolvent *via* sonication, which, besides our studies of disaggregation by adding a second nonpolar-antisolvent (see DLS results), could be relevant for future studies using nonpolar-antisolvents having however similar net-basicity values.

3.3. Fourier transform infrared (FTIR) spectroscopy

Fig. 1 shows the FTIR absorption spectra (in the wavenumber range 3800–800 cm^{-1}) of: THF alone (*versus* air as blank), un-sonicated MCC powder (*versus* a dried KBr crystal as blank), cellulose-THF (0.5 mg/mL) (*versus* THF as blank), and a cellulose drop-casted films (*versus* the underlying Si/SiO_2 surface as blank).

Overall Fig. 1 shows that in all the spectral range the MCC powder and the drop-casted film from the suspension in THF are practically identical (subtle differences due to crystallinity are discussed ahead). This is in agreement with previous reports showing identical FTIR spectra between cellulose treated with different physical–chemical treatments and the starting materials, for example amorphous cellulose obtained by milling MCC;(Wan Ishak, Rosli, and Ahmad 2020) NC

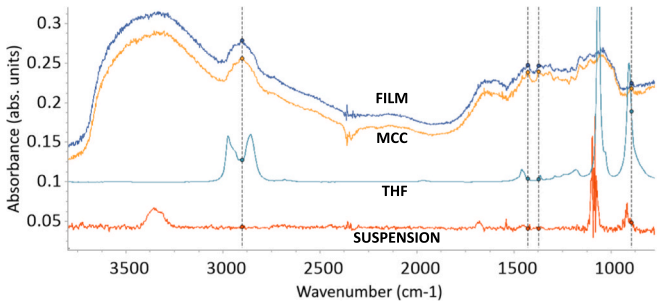

Fig. 1. FTIR absorbance spectra (as labelled) of THF, MCC powder, cellulose suspension in THF (at 0.5 mg/mL) and drop-casted film, in the wavenumber range 3800–800 cm^{-1}. Dashed vertical lines indicate the wavenumbers 2900, 1430, 1372 and 893 cm^{-1} (as displayer by the Spectragryph freeware) used to estimate the Nelson & O'Connor crystallinity indexes Cr.R1 (1372 cm^{-1}/2900 cm^{-1}) and Cr.R2 (1430 cm^{-1}/893 cm^{-1}). [113].

obtained from soybeans *via* different levels of ultrasound or high-pressure homogenization treatments; [143] CFs extracted after chemical (KOH) treatment and freeze drying of CNFs; [145] CNCs after being sonicated; [148] NC fibers and grass wastes treated with sodium NaClO; [3] or CNCs obtained from different sources.(Chhavi [135,116,102,121] Please notice that to our knowledge, only complex reactions during sonication-assisted *enzymatic* hydrolysis generate changes in the FTIR spectral features, see *e.g.* [26].

In more detail: Fig. 1 shows that both the MCC powder and the cellulose film generate a FTIR band in the 3400–3260 cm^{-1} spectral region (centered ≈ 3350 cm^{-1}), which in turn is not present in the spectrum of the THF alone. Besides indicating water content in the sample, bands between 3700–3200 cm^{-1} are assigned to three types of H-bonding in cellulose: O(2)H-O(6) intramolecular, O(3)H-O(5) intramolecular, and O(6)H-O(3) intermolecular. [75] In regard to other characteristic cellulose bands, Fig. 1 shows bands around 2924 cm^{-1} from MCC and drop-casted films, previously used to distinguish between C-H signals with aid of the fingerprint region between 2000–600 cm^{-1}; (Shi, Xing, and Lia 2012) at around 1426 and 895 cm^{-1}, used previously to analyze crystallinity changes with the method by Nelson & O'Connor; [85,113]also a band centered around 1640 cm-1, associated with O-H bonding [51] and water content of cellulosic materials, [72] (M.-F. [152] particularly the bending mode; [98,8]and also a band around 1430 cm^{-1}, associated with –CH_2 bending at C6; [123,51]a band centered around 1050 cm^{-1}, associated with C–H vibration and β-glycosidic linkages. [51].

Thus, because of the nearly identical nature between the spectra of MCC and the film obtained drop casting the suspension in THF, it is reasonable to state that the narrow character of the band generated by the suspension in THF at around 3300 cm^{-1} (Fig. 1) is not caused by structural changes in the cellulose in suspension, neither a smaller intermolecular H-bonding network, [123]but because of detection limitations due to low concentration.

In regard to changes in crystallinity due to sonication, Fig. 1 shows that the absorption spectra of MCC and film are closer to each other at 1430 cm^{-1} than at 2900 cm^{-1}. This is in agreement with the literature, which reports that larger absorption values at ~ 1429 cm^{-1} indicate a larger crystallinity. [113] This is clearer when using the crystallinity indexes of Nelson & O'Connor Cr.R**1** = A_{1372}/A_{2900} and Cr.R**2** = A_{1430}/A_{893}. [113] Inserting the absorbance values of the MCC and film spectra in these ratios are obtained the values $Cr.R1_{MCC}$ = 0.2178/0.2553 = 0.853 and $CrR1._{FILM}$ = 0.2243/0.2774 = 0.809, respectively. Thus, according to the Cr.R1 ratio, the cellulose in the drop-casted film is (0.809/0.853) 5.2 % less crystalline that in the MCC powder, while the Cr.R2 ratio suggests that the cellulose in the film is the same to that in the MCC (see Table S-1 in the Supplementary File). Since the bands used in Cr.R1 relate to C-H bending (~1372 cm^{-1}) and C-H stretching (~2900 cm^{-1}) vibration bands, while the bands used in Cr.R2 relate to asymmetric CH_2 bending ("crystallinity band", ~1430 cm^{-1}) and C-O-C stretching of the β(1,4)-glycosidic linkages ("amorphous band", ~898 cm^{-1}), [113] our results suggest that 15 min of sonication decrease crystallinity mainly by modifying the vibration bands of the C-H groups in the β(1,4)-D-glucopyranose units, while barely modifying the CH_2 and C-O-C groups. Thus, overall our results suggest that (i) sonication during 15 min in THF causes a decrease in crystallinity of 5 %, (ii) mainly related with changes in H-bonding than with changes in the DP values. The results reported by Mattonai et al. using the same MCC [85] support this assumption, since that investigation reported that milling causes an important decrease in the Cr.R**2** = A1430/A893 index. Since milling is much harsher than sonication in THF, which would cause an important change in the signals related to the C-O-C stretching of the β(1,4)-glycosidic linkages.

Thus, from the network of noncovalent interaction forces present in cellulose (described in the introduction section) constituted by H-bonds (between the –OH hydroxyl groups at C2, C3, and C6 of the monomers, [14] and also van der Waals (vdW) interactions)(Paulsen [106] which together with the stiffness of the glycosidic linkage, generate crystalline domains),(Mariano, Kissi, and Dufresne 2014) sonication in THF seems to not affect the latter. In other words, the decrease in crystallinity seems to be mainly caused by a disruption of the H-bonding and VdW networks instead of breaking the polymeric chains, which is reasonable because of the low sonication energy and the nonpolar-antisolvent nature of THF.

Thus, despite that in principle, after the high reactivity of the amorphous regions within MCC, and also the low energy related to sonicating it in a nonpolar-antisolvent during 15 min at 40 kHz/70 Watts, should release mainly amorphous cellulose, our FTIR results suggest that after sonication in THF, there are obtained particles *constituted by amorphous cellulose and also crystalline material.*

Interestingly, according to literature, NC materials are obtained *via* ultrasound only when it is coupled with acid or enzymatic hydrolysis, [55] which are much harsher conditions than those provided by THF. Further quantitative studies on the effect of sonication on the values of CI or DP (*e.g.* similar to the study by Mattonai et al. [85], are above the scope of the present work (and indeed constitute part of its future perspectives), however our analyses and conclusions hold despite the specific extent of crystallinity/amorphicity of the material, because both types have –OH groups exposed, capable of interacting with THF or $CHCl_3$.

Finally, please notice that the spectra of MCC and drop-casted film show a *barely* defined FTIR band at around 2200–1900 cm^{-1}, which can be reasonably attributed to impurity traces in the commercial MCC used in the present work, as it has been observed in at least one reference using MCC from Sigma.(H. [149] However, since such a band has been also observed in the spectra from extractives of cellulosic materials (*e.g.* (Md Salim, Asik, and Sarjadi 2021), a further analysis is provided here. In regard to lignins, bands at 2129 and 2019 cm^{-1} are assigned to C=C stretch vibration of the lignin aromatic ring. However, the spectra in Fig. 1a,b does not show several other bands that are also associated with lignin, such as those around 1750–1500 cm^{-1} from aromatic skeletal vibration [146,29]nor those at 1611 cm^{-1} from the aldehyde group in lignin, nor at 2350 cm^{-1}, associated to the presence of carbon dioxide. [2]Furthermore, in the fingerprint region are not observed complex bands in the 1515–1505 cm^{-1} region from aromatic skeletal vibrations. [58] Besides lignins, hemicelluloses, oxycelluloses and furans are impurities also commonly found in MCC.("MicroCrystalline Cellulose Chemical Characterization Services," n.d.) In this regard, Fig. 1a,b does not show bands from carbonyl groups with oxidized cellulose, at 1740 cm^{-1}, [18] (Y. [140]or 880 cm^{-1}, [18]Thus, it is reasonable considering that the band band at around 2200–1900 cm^{-1} is caused by impurity traces that are negligible in comparison with the clear and typical cellulose spectral features from the MCC starting material and the amorphous cellulose present in THF after sonication/filtration.

3.4. Computational complementary analyses

Besides confirming the presence of cellulose in THF with FTIR, complementary qualitative computational studies were used to further rationalize the formation of suspensions in THF but not in CHCl3. Fig. 2 shows the DFT optimized syn cellobiose dimer and the cellobiose-THF, in vacuum. Figure S-1 in the Supplementary File shows the optimized complexes of cellobiose with $CHCl_3$, water, methanol and AcO-. The characteristic lengths of intra-molecular interactions (HINT1, HINT2) and that formed with the solvents or anion (HEXT1) are resumed in Table 2. The calculated total electronic energies (E, in Hartree), enthalpies (H, in Hartree), Gibbs free energies (G, in Hartree), and entropies (S, cal/mol•K) for optimized equilibrium model structures are shown in Table 3.

Considering the lengths and angles generated in the cellobiose optimized geometry as being unaltered due to the presence of any external molecule, the data in Table 1 (extracted from Fig. 2 and S-1) shows that: the presence of $CHCl_3$ barely modifies the lengths of HINT1 and HINT2, and also the angle of HINT2, while the angle of HINT1 remains indeed unchanged. On the other hand, water, methanol and the acetate anion decrease the length of HINT1 from 2.628 in cellobiose alone, to values below 2 Å, while THF decreases this length to 2.1 Å. The same trend is observed in regard to the angle of HINT1, with water, methanol and acetate modifying this angle to values above 163.5°, and THF causing a smaller change of 158.6°. As shown in Table 2, the exact same trends are observed for the lengths and angles of HINT2 in presence of the solvent or anion molecules, with the acetate anion generating the shortest length of the interacting bond with cellobiose (1.586 Å). These *qualitative* results clearly show the lack of interaction between the acidic proton in $CHCl_3$ and the cellobiose dimer. Moreover, a shorter length of H-bonds with cellobiose referred to a better solubility of cellulose in the ionic liquids, and also confirmed the premise of the cellulose dissolution that the hydrogen bond formed between ionic liquid and cellulose must be stronger than the intramolecular H-bonds of cellulose. (X. [82]Thus, in agreement with the gravimetric results, the results of DFT calculations reveal that the supramolecular association of cellulose with THF is indeed thermodynamically favorable ($\Delta G = -20.9$ kJ/mol), whereas supramolecular association of cellulose with $CHCl_3$ is unprofitable ($\Delta G = 8.1$ kJ/mol) in terms of calculated Gibbs free energies of reaction. Table S-2 shows the calculated total electronic energies (E, in Hartree), enthalpies (H, in Hartree), Gibbs free energies (G, in Hartree), and entropies (S, cal/mol•K) for optimized equilibrium model structures. In regard to the noncovalent interactions (NCI) analysis, Figure S-1 in the Supplementary File shows the intermolecular interactions in the optimized equilibrium model supramolecular associates cellobiose···THF and cellobiose···$CHCl_3$, NCI shows a stronger interaction with the –OH groups in cellobiose than those present when interacting with $CHCl_3$.

Overall the qualitative computational results indicate a thermodynamically unprofitable interaction between the cellobiose dimer and $CHCl_3$, while THF generates values that indicate such an interaction is indeed possible, in some cases in a similar fashion to the interactions generated with polar solvents and anions. This is in agreement with our experimental results, which shows that the highest net-basicity of THF increases the interactions with the –OH groups, which behave as acids, while $CHCl_3$ presents weaker interactions despite the hydroxyl groups in cellulose as mainly as bases.

3.5. Atomic force microscopy (AFM)

Fig. 3 shows AFM micrographs of drop-casted cellulose surfaces from THF onto Si/SiO_2 at different scales ranging from 4 to 0.4 μm. As discussed in the DLS results ahead, the R_h values estimated are similar to previous works obtained using the same pore filter cutoff to filter CNCs. (Y. [57,16,62] In this regard, Fig. 3 shows that regardless the scale, the micrographs in Fig. 3 do not show the presence of structured materials such as crystals or fibers, in scales ranging from 4 to 0.4 squared microns. Instead, at larger sizes are observed globular, irregular structures, while at lowers sizes is observed the presence of material, however without showing any crystalline or fibrillar structure. These results are completely different to those from cellulosic materials obtained previously using *sonication-assisted* methods (at scales similar to those in Fig. 3), such as MCC,[141]NC,[65,143,41]NCC,[137,26,78]CNCs, [125,148] (Di [30,62,102,116,16,132,101] (Chhavi [135,53] spherical CNCs, [25] functionalized CNCs, [144]CNFs,[3,145] nano whiskers, (Nascimento et al. 2015) and BC fibrils. [107].

Of course "absence of evidence does not mean evidence of absence", particularly when considering the crystallinity estimated using the Nelson & O'Connor indexes which suggests that after sonication in THF, there are obtained particles constituted by amorphous cellulose and also crystalline materials, which would aggregate/agglomerate into the globular structures observed in Fig. 3. However please notice that obtaining spherical cellulose particles is not trivial as it requires a *shaping* step after cellulose regeneration, as reviewed by Carvalho et al. [20] Thus the globular structures shown in Fig. 3 could be explained to form after of the relatively large surface energy of the silicon substrate,

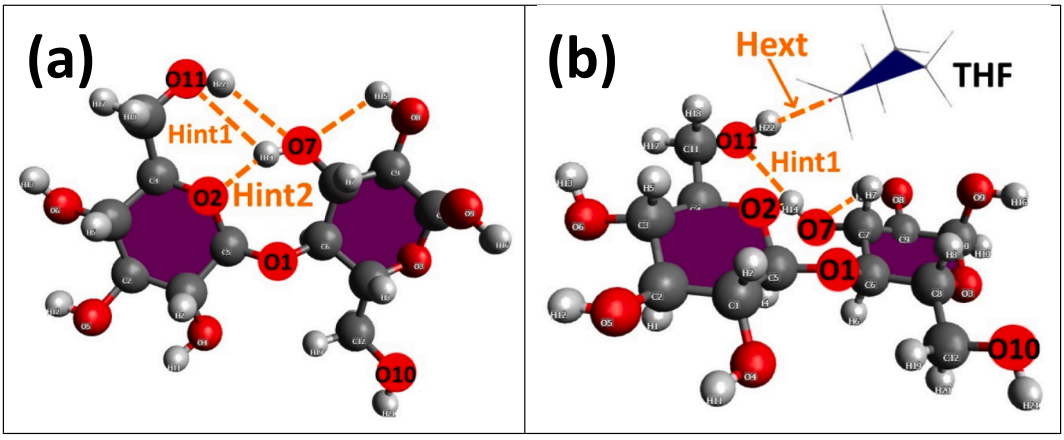

Fig. 2. (a) syn cellobiose dimer optimized at the ωB97XD level (after an optimization at the M06-2X level), [92]) showing the intra-molecular bonds $H_{INT}1$ and $H_{INT}2$ (under a cutoff of 2.7 Ã…; and (b) cellobiose-THF complex optimized at the ωB97XD over the pre-optimized cellobiose dimer in "a", showing the noncovalent bonding stablished between cellobiose and THF ($H_{EXT}1$). For easier visualization: some characteristic oxygens are enhanced with a larger font, rings (from glucose and THF) are highlighted with color, and THF is shown with a wireframe. (For the complexes between cellobiose and $CHCl_3$, water, methanol and AcO- please see Figure S-1).

Table 2
Intra-molecular cellobiose bonds (HINT1 and HINT2) lengths (in Å) and angles for the simulated systems, together with the complex cellobiose-solvent (or −anion) bond length (HEXT1) for the simulated systems.

System	$H_{INT}1$ (H14···O11) Length	Angle*	$H_{INT}2$ (H14···O2) Length	Angle†	H_{EXT} Cellob(H22)···SOLV Length	Angle‡
Cellobiose	2.628	124.7	1.848	158.4	–-	–-
Cellob···THF	2.116	158.6	2.172	122.6	1.765	171.2
Cellob···$CHCl_3$	2.362	124.7	1.854	156	2.9¶	72.8¶
Cellob···Water	1.98	164.1	2.48	101.7	1.845	160.3
Cellob···MetOH	1.87	167	2.367	105.8	1.753	170.5
Cellob···AcO^-	1.912	163.5	2.155	116.3	1.586	167

* O7-H14···O11.
† O7-H14···O2.
‡O11-H22···Solvent.
¶ Considering the interaction between O11 from cellobiose (acting as a Turbak base) and the acidic H in $CHCl_3$.

Table 3
Calculated values of Gibbs free energies of reaction (ΔG in kJ/mol) for model processes.

Model process	ΔG
Cellobiose + THF → Cellobiose···THF	**−20.9**
Cellobiose + $CHCl_3$ → Cellobiose···$CHCl_3$	**8.1**
Cellobiose + Water → Cellobiose···Water	−15.5
Cellobiose + Methanol → Cellobiose···Methanol	−26.3
Cellobiose + AcO^- → Cellobiose···AcO^-	−120.9

as it has been reported in a study on PMMA (a linear unbranched homopolymer, similarly to cellulose). [48] In such study, the size of the aggregates increased with the PMMA concentration and was always larger than the size of the aggregates in solution measured by DLS. In regard to the latter, the globular aggregates in Fig. 3, within the microns range, are indeed larger than the DLS estimations (R_h ~ 255 nm, see details in the DLS section next).

3.6. *Dynamic light scattering (DLS)*

Fig. 4 shows R_h distributions (a, b) and intensity autocorrelation function decay curves (c, d) generated by either the cellulose suspensions in pure THF (*i.e.* $X_{CHCl3} = 0$) at three concentrations (0.5, 0.25, and

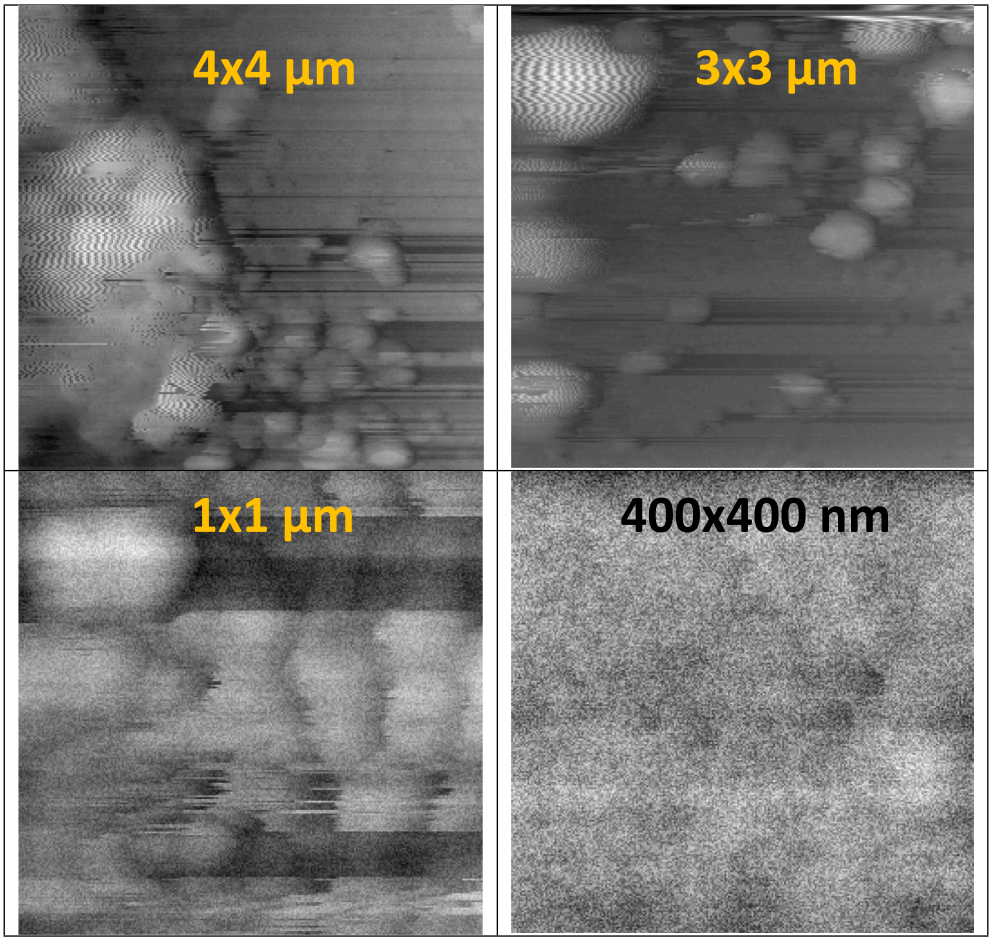

Fig. 3. Typical height AFM micrographs of the drop-casted cellulose at different scales, as shown.

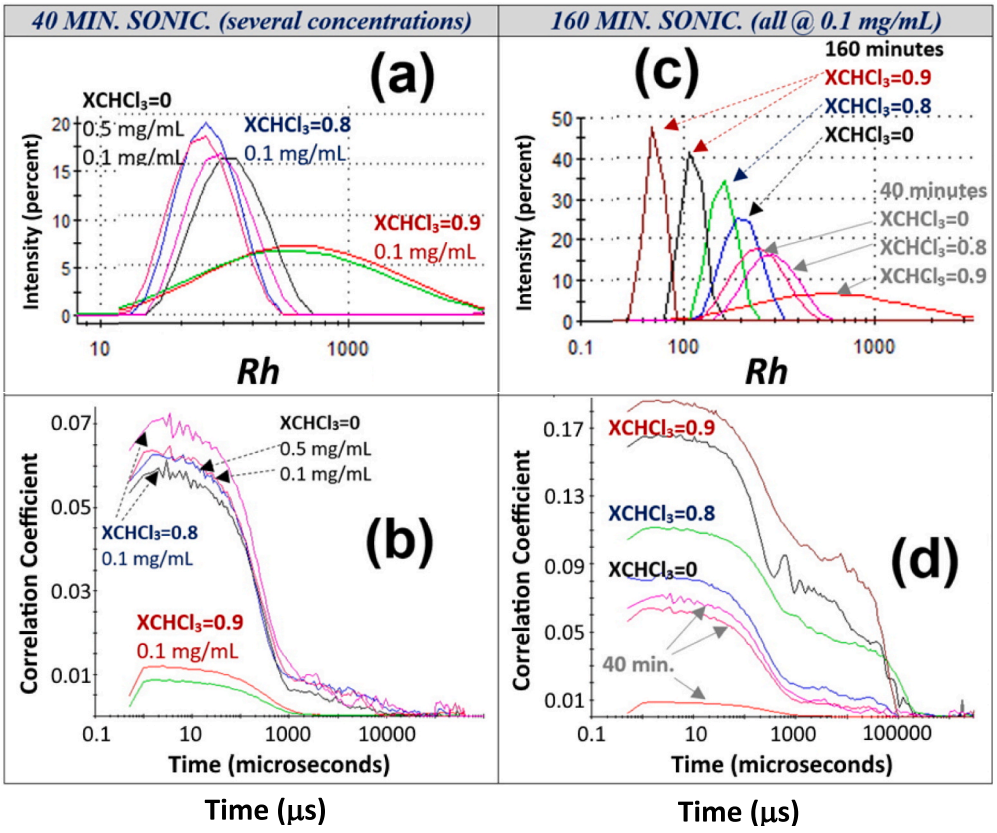

Fig. 4. (a, c) Typical hydrodynamic radius (R_h) profiles; and (b, d) correlation function plots; of cellulose suspensions in THF alone (*i.e.,* $XCHCl_3 = 0$) or in the solvent mixture THF-$CHCl_3$ ($XCHCl_3 = 0.8$ or 0.9) at different concentrations, after 40 or 160 min of sonication (as shown). In "c" and "d" the data obtained after 40 min of sonication (*i.e.* that shown in "a" and "b") is also shown for comparison purposes.

0.1 mg/mL), or by the suspensions in THF-$CHCl_3$ mixtures (*i.e.* $X_{CHCl3} = 0.8$ & 0.9), at 0.1 mg/mL, either after the original 40 min of sonication, or after adding 120 min (for a total of 160 min of sonication) to the filtered suspensions.

Fig. 4a shows that regardless the concentration (0.1 or 0.5 mg/mL), the samples in pure THF ($X_{CHCl3} = 0$) generate an average $R_h \sim 255$ nm with a size distribution ranging between 140–460 nm. These dimensions confirm the assumption sketched in the gravimetry results section, about having a *suspension* in THF after sonication/filtration. In principle, the 0.45 μm filter membrane should generate particles with maximum R_h values close to 450 nm, however, it is known that reactions such as aggregation of adsorbed natural organic material is one of the known drawbacks of filtration. [35].

The particle average $R_h \sim 255$ nm is within the range of different R_h estimations from *structured* materials (*e.g.* crystals or fibers) obtained from different raw materials and treatments, such as Rh ~ 50–200 nm from NCC; [137,78,144]Rh ~ 60–400 nm from CNCs;(Di [30,121,125,65,101] (Chhavi [135]$R_h \sim 260$ and 150 nm from functionalized CNCs; [132]$R_h \sim 100 <$ to 260 nm from CNFs; [105,145,107,121]or Rh ~ 200–400 nm from NC; [143]and Rh ~ 100–300 nm from cotton fibers.(Nascimento et al. 2015) (All of the references cited here confirmed the presence of structured materials (crystals or fibers) using microscopy techniques). The similarity between our results and the cited literature in regard to the R_h value can be explained by the use of membranes with a pore size cutoff of 450 nm, which has been used previously used to filter CNCs.(Y. [57,16,62]For example, Hu and Abidi fractionated particle size distributions of size-unified CNCs ranging in 9 − 1700 nm, by using membranes with cut-off values of 220, 450 and 800 nm.(Y. [57] In regard to the correlation coefficient values, Fig. 4b shows that all the $X_{CHCl3} = 0$ samples generate the same the decay time (≈ 100 K μs) because of having similar average particle sizes. The samples also generate similar decay steepness, which suggests that changes in concentration do not generate important changes in the size-polydispersity of the samples, because it is known that size-monodisperse samples generate steeper decays.("Dynamic Light Scattering: An Introduction in 30 Minutes" 2014)) [64,142,108,27].

The fact that the 0.1 and 0.5 mg/mL suspensions in THF generate similar R_h values, suggest a limiting particle size in equilibrium with THF and neighboring particles, without precipitating into larger aggregates/agglomerates when hydrodynamic volumes of the polymers overlap, leading to uncontrolled precipitations, as observed previously when monitoring the *specific viscosity* (not particle size) of cellulose diacetate pure granules in THF. [110] This explanation holds for previous studies on gelsolin, for which it was also observed the presence of the same Rh value however different intensity values, which was explained to be caused by the formation of "reclusive oligomers" [9] having the same particle size regardless larger concentrations.

The DLS data generated in the present work shows that for larger R_h values the intensity decreases (see Fig. 4a). This trend is opposite to that observed during the process of nucleation of gelsolin cited here. [9] Thus, our data shows that concentration does not change the R_h value, suggesting some sort of reclusive nucleation, different from uncontrolled precipitation, which would lead to fibrillar structures. The data obtained in presence of the purely acidic antisolvent $CHCl_3$ provides further understanding on this.

3.7. Disaggregation in suspension

Fig. 4a shows that the suspensions in mixed solvent with 80 % v/v of $CHCl_3$ ($X_{CHCl3} = 0.8$), generate an average value R_h of ~ 320 nm, which is 25 % larger than that from the 0.1 mg/mL $X_{CHCl3} = 0$ suspensions,

while the $X_{CHCl3} = 0.9$ suspension generate $R_h \sim 610$ nm, which is 145 % larger than $X_{CHCl3} = 0$ suspension, generating also a much broader distribution of particle sizes, indicating a higher dispersity. In regard to the correlation coefficient, the $X_{CHCl3} = 0.9$ suspensions generate much smaller values, with decay times 2 orders of magnitude smaller than those of the $X_{CHCl3} = 0$ & 0.8 samples, which in turn are similar between each other.

3.8. Disaggregation on the surface of water (Langmuir trough experiments)

In regard to the increase of the particles in suspension because of $CHCl_3$, Figure S-3 shows that the film spread from the suspension in THF alone ($X_{CHCl3} = 0$) occupies around 10 % of the total surface area in the instrument, while films obtained by dropping the $X_{CHCl3} = 0.8$ & 0.9 suspensions occupy around 30 and 60 %, indicating disaggregation of the particles standing onto the surface of water (in the case of the $X_{CHCl3} = 0.9$ film, it generates aggregates with the largest surface areas despite having half of the surface concentration than the $X_{CHCl3} = 0$ film). On the other hand, Figure S-4 shows that the $X_{CHCl3} = 0$ & 0.8 films have a clearly different morphology. The fact that even onto the surface of water the $CHCl_3$ has a disaggregating effect provides further evidence that the disaggregation in suspension observed by DLS is not caused by possible moisture THF and $CHCl_3$, simply because in presence of water any possible "drying" effect by $CHCl_3$ should be nullified, and the aggregation observed in the air/water interface should be minimized. However our results show that the disaggregating effect of $CHCl_3$ is even larger. Furthermore, relaxation surface pressure curves (holding the device barriers and recording the change in surface pressure, which reflects internal molecular rearrangements within the Langmuir films) show identical kinetics between the $X_{CHCl3} = 0$ & 0.9 films (results not shown), indicating that any possible moisture in THF, which could be dried by $CHCl_3$, is not the cause of the disaggregative effect of $CHCl_3$.

3.9. The role of cosolvency during the disaggregation of the cellulose particles

Continuing with the DLS analyses, despite our gravimetry results show that it is not possible generating suspensions *via* sonication in the nonpolar-antisolvent $CHCl_3$ (a trend also observed in our qualitative computational complementary analyses), it is indeed possible having suspensions in a media with 10 % THF and 90 % $CHCl_3$ ($X_{CHCl3} = 0.9$). This is relevant because (i) in order to obtain dispersions of NC in a nonpolar solvent such as $CHCl_3$ it is mandatory to perform a solvent exchange process, as previously done when starting from acetone (polar aprotic with a dielectric constant of 21);(Indarti, Marwan, and Wan Daud 2020) and (ii) our results indicate the occurrence of a *cosolvency* effect, where a mixture of two poor solvents or antisolvents for a polymer provides a medium that acts as a good solvent, [46] −or at least relatively better solvent, in our case-.The extent of increase in R_h due to the presence of $CHCl_3$ observed in the present work (145 %), is over 5 times larger than the 28 % increase in Rh reported by Peesan et al. [109] using hexanoyl-chitosan, with R_h values of 38.5 and 39.9 nm in THF and $CHCl_3$ respectively, which the authors rationalized to be caused by a freer chain expansion occurring in $CHCl_3$. The smaller extent of increase in $CHCl_3$ reported by these authors can be explained by the hexanoyl functionality in their solute, which is expected to decrease the effect of solvent acidity/basicity, after the presence of stronger dispersive interaction forces. A good limiting case of this is the work by Cametti et al., [19]for polyphenylacetylene (PPA), which generated similar $R_h \sim 260$ nm in THF, $CHCl_3$ or toluene, because of the effect of the phenyl units decreasing the relevance of acid-base interactions. In resume, these contributions show that for molecules including hydrophobic functionalities, THF and $CHCl_3$ become comparable due to similar polymer expansion, after acid-base interactions become less relevant.

Thus, after the work by Peesan et al. [109], and also because of the well-known fact that cosolvents are more effective in expanding the polymer coil than increasing temperature, with mixtures of two poor solvents or antisolvents for a polymer providing a medium that acts as a good solvent, [46]our results suggest that despite the antisolvent nature of $CHCl_3$ for cellulose, when it is added to the nonpolar environment of the suspensions in THF, it behaves as a *cosolvent* as it effectively induces disaggregation/deagglomeration. (Please notice that if $CHCl_3$ would promote further aggregation, it would be labelled a "cononsolvent" [46] (or co-nonsolvent, or co-antisolvent, or co–/antisolvent, all terms used in the literature)).

This aspect may be exploited in future investigations focusing on the exchanging of solvent and antisolvent, (El Seoud, Omar A. et al. 2019; [79,10] and diffusive processes [79] to reestablish inter- and intramolecular H-bonds [10] mentioned in the introduction section, however, under null polarity. This has not been explored in the literature to the best of our knowledge.

Another set of (bibliographic) studies on supramolecular properties of polymers using THF and $CHCl_3$ are those by Bistac and co-authors, [12,13]focused on the disaggregation of stereoregular PMMA (a linear unbranched homopolymer, similarly to cellulose) dissolved in THF and disaggregated by adding $CHCl_3$, The authors sketched that the formation of PMMA aggregates depends, among other parameters, on the development of acid-base interactions between PMMA chains and the solvent molecules, analyzing the results in terms of the so-called *complexing power* of the solvents, in turn correlating it to their acid-base character. PMMA has a basic nature due to its ester functional groups with a carbonyl oxygen atom. On the other hand, the acidic (H-bonding donor) hydrogen atom in $CHCl_3$ promotes strong acid-base interactions with PMMA, forming acid-base complexes between the ester basic group of PMMA and the hydrogen acid atom of $CHCl_3$. Such acid-base interactions then become comparable to the hydrophobic interactions, thus helping to hinder the formation of chains aggregates, promoting disaggregation *via* Lewis acid-base PMMA-$CHCl_3$ interactions that are stronger than the inter- and intra-molecular PMMA-PMMA interactions, driven by the poor solute–solvent interactions in THF. The cited authors did not take into account steric effect and macromolecular conformations of aggregates, [12]however, the similar molar volumes of THF and $CHCl_3$ (see Table 1) suggest that steric effects are not critical. Regardless, following these contributions, it is reasonable to propose qualitatively, that because of the relatively high Kamlet-Taft net-basicity of the nonpolar-antisolvent THF (similar to ILs and DESs used in the context of cellulosic materials), and also the energy input of 40 kHz/70 Watts sonication, the interaction between THF and the –OH groups in the anhydroglucose units, acting as Turbak acids (H-bonding donors) becomes thermodynamically possible (which is in agreement with DFT qualitative analyses in vacuum). Such cellulose-THF interaction however is weak, due to weak solute–solvent interactions in the nonpolar-antisolvent THF, generating cellulose aggregates after the formation of inter- and intra-molecular cellulose H-bonds. However, because of the ability of the –OH groups in cellulose to behave as Turbak bases, adding the Kamlet-Taft purely acidic $CHCl_3$ cause disaggregation by overcoming polymer–polymer interactions via the formation of Lewis acid-base complexes between the hydrogen atom of $CHCl_3$ and the –OH groups in the anhydroglucose units, together with the discussed cosolvency effect.

Please notice that the works cited here, by[12,109]and[19] can also be satisfactorily explained in terms of Kamlet-Taft acidity/basicity (similarly to examples provided in Section S-1.1. in the Supplementary File).

Detailed studies on cosolvency lie out of the scope of the present work, since those require evaluating its effect on parameters such as viscosity, similarly to previous works with PMMA in binary solvent mixtures of ACN with pentylacetate or 1-butanol.[46].

3.10. Excess sonication

Since crystalline regions are known to degrade when using high temperatures such as 80 °C [3] or long-time ultrasonic treatments. [26,148,141,6] (reason why deagglomeration is one of the main roles of ultrasound used in the treatment of NC materials), [55] in the present work the stability of the suspensions was tested by adding 120 min of sonication to the samples, which in turn also causes an increase in temperature (from 25 to 40 °C), in order to obtain further information on the cellulose particles in THF or THF-$CHCl_3$.

Fig. 3c shows that after the extra sonication, the sample without cosolvent ($X_{CHCl3} = 0$) generates an $R_h = 200$ nm, which is 25 % *smaller* to that of the samples sonicated 40 min (255 nm), suggesting that larger sonication energy and thermal energy cooperate in breaking the aggregates of cellulose. When the chemical energy (orthogonal Lewis properties) provided by $CHCl_3$ is added, R_h decreases by 44 % (from ~ 320 nm to ~ 180 nm) in the $X_{CHCl3} = 0.8$ suspension, and by 85 % (from ~ 610 nm to ~ 90 nm) for the $X_{CHCl3} = 0.9$ suspension. In all cases, the values of the correlation coefficient and decay times *increase*, further indicating the presence of smaller particles (Fig. 3d). For nanoparticles in general, poor solute–solvent interactions can generate either *aggregates* and/or *agglomerates*, depending if the interparticle forces are strong (*e.g.* formed during synthesis), or loose (can barely withstand external stress), respectively. [118] A good example to differentiate between aggregation and agglomeration of CNCs, is that reported by Chang et al., [23] in which adding a *polar* cosolvent (DMF) to aqueous suspensions of CNCs (which are aggregated, due to the nonsolvent nature of cellulose for CNCs), causes a *decrease* in the R_h values. This result, opposite to our results, indicates that for structured materials such as CNCs, improved cellulose-solvent interactions lead to an increase in the number of *single CNCs* with smaller Rh values than agglomerated CNCs.

As proposed in our DLS results, in the case of polymers, improved solute–solvent interactions causes the swelling of the aggregates, increasing the R_h values. Since the AFM micrographs of drop-casted $X_{CHCl3} = 0$ suspensions (Fig. 3) do not show evidence of any type of structured material, and also, since the thermal or mechanical force required to break polymeric cellulose chains is much larger than that of sonication at ~ 40 °C, our results under excess sonication suggest that the aggregates of cellulose obtained in THF are indeed formed by *agglomerated aggregates*: small aggregates of crystalline and amorphous cellulose linked in turn *via* H-bonding when interacting with antisolvents, which cannot keep bonded after increased sonication time and temperature. The polydispersity of R_h values could correlate with different polymeric lengths. This simple DLS criterion could be a simple way to distinguish between polymeric cellulose and cellulose nanoparticles, and to our knowledge has not been reported in the literature.

4. Conclusions & future perspectives

This work reports the production of suspensions of cellulose in the purely basic nonpolar-antisolvent THF by means of sonication with frequency and power of 40 kHz and 70 Watts respectively. Sonication allows generating suspensions in-situ in THF in a single operation, differently from methods involving milling of MCC and then stirring in the selected solvent. Under sonication-assisted conditions, the physical–chemical properties of cellulose (capabilities to behave as a Turbak acid, high reactivity of amorphous regions), and THF (low viscosity and surface tension, high *net-basicity* and molar volume) interact in a cooperative manner to generate the suspensions of cellulose in a nonderivatizing nonpolar-antisolvent such as THF. The role of the relatively large positive net-basicity of THF was demonstrated by the *purely acidic* $CHCl_3$, which despite having similar molar volume, viscosity and surface tension than THF (the latter two improving ultrasonic cavitation), has a negative value of net-basicity, compromising the production of sonication-assisted suspensions, despite cellulose has shown to behave as a (Turbak) base in polar media. (Complementary qualitative computational DFT in vacuum, and NCI analyses also show that THF is thermodynamically favorable over $CHCl_3$). Because of the membrane cutoff values selected as an effective and simple fractionation method, the particles in THF are within the range of previously reported cellulose particles. FTIR spectroscopy indicates that the cellulose in the THF suspension after sonication is around 5 % less crystalline than the starting MCC material. The results of the experiments of disaggregation using the nonpolar-antisolvent $CHCl_3$ (in suspension and using Langmuir films on the surface of water), together with the incapability of $CHCl_3$ alone to generate suspensions, provide evidence of the occurrence of a cosolvency effect (instead of cononsolvency) under nonpolar conditions when using $CHCl_3$ as a second antisolvent. This is relevant because shows that cosolvency can be exploited to generate processes analogous to solvent exchange procedures, for example, in order to obtain dispersions of NC in a nonpolar solvent such as $CHCl_3$ it is required a solvent exchange process from acetone (polar aprotic; dielectric constant of 21) into nonpolar $CHCl_3$. (Indarti, Marwan, and Wan Daud 2020) These results also demonstrate that the net-basicity (estimated from Kamlet-Taft, or other solvent scales such as Gutmann) overall shows to be a complementary descriptor to other scopes such as *e.g.* the complexing power discussed before by [12,13]. Our results suggest that the purely acidic character of $CHCl_3$ would then cause disaggregation by overcoming polymer–polymer interactions via the formation of Lewis acid-base complexes between the hydrogen atom of $CHCl_3$ and the –OH groups in the anhydroglucose units (acting as Lewis bases) and the acidic hydrogen in $CHCl_3$. Such interactions however are only possible in presence of THF, demonstrating the role of cosolvency. Excess sonication experiments suggest that the particles observed in THF are indeed agglomerates of aggregates: small aggregates of cellulose linked in turn *via* H-bonding when interacting with antisolvents, which cannot keep bonded after increased sonication time and temperature, the polydispersity of R_h values could correlate with different polymeric lengths. This simple DLS criterion could be a simple way to distinguish between polymeric cellulose and cellulose nanoparticles.

To the best of our knowledge our scope has not been reported in the literature. Thus, the suspensions in THF and also those in mixed THF-$CHCl_3$ binary systems could present a novel platform to perform studies on the dissolution/regeneration of cellulose, by performing different studies, using proper chemical probes (*e.g.* ILs or DESs), substrates and matrices, under purely Lewis acid-basic interaction forces in nonpolar media, and also appropriate physical methods and analytical approaches in order to analyze systematically the regeneration processes and rationalize new methods for gaining insight in mechanics useful to get precise control of supramolecular structures (for example, focusing on the exchanging of solvent and antisolvent), using appropriate experimental and/or complementary computational methods, taking advantage of an environment with limited forces of interaction by using the nonpolar-antisolvent approach, evaluating correlations with solvent parameter scales when possible. Please notice that these possibilities are also extensive to polymers different from cellulose, as shown by the examples cited in the present work.

CRediT authorship contribution statement

Sergio E. Domínguez: Writing – original draft, Validation, Resources, Methodology, Funding acquisition, Data curation, Writing – review & editing, Visualization, Supervision, Project administration, Investigation, Formal analysis, Conceptualization. **Alexander S. Novikov:** Supervision, Methodology, Formal analysis, Conceptualization, Validation, Resources, Investigation, Data curation. **Dmitry A. Kornilov:** Investigation. **Antti Vuolle:** Investigation. **Mia Meriläinen:** Investigation. **Hiram Isaac Beltrán:** Supervision, Methodology.

Declaration of competing interest

The authors declare that they have no known competing financial

interests or personal relationships that could have appeared to influence the work reported in this paper.

Acknowledgments

Sergio E. Domínguez acknowledges the Mexican National Council for Science and Technology (CONACyT) for the scholarship N°. 310828. From the University of Turku are acknowledged Pia Damlin for donating MCC and facilitating access to the DLS instrument; and also Ermei Mäkiläa and Martti Kaasalainen for their support such instrument. From Malvern Instruments Ltd. to Michael Kaszuba because of his technical support in regard to the use and interpretation of the DLS instrument, and also for suggesting the respective experimental/analytical approach. From Universidad Autónoma Metropolitana are acknowledged Sergio Revah Moiseev and José Campos Terán for giving access to the Langmuir trough instrument.

Alexander S. Novikov is grateful to the RUDN University Scientific Projects Grant System, project N° 021342-2-000.

Dmitry A. Kornilov is grateful to Eurasian Scientific and Educational Center (No. TsPD-ML-4/RF-23) and the Ministry of Science and Higher Education of the Russian Federation (No. FZWU-2023-0002)

References

[1] S. Acharya, S. Liyanage, P. Parajuli, S.S. Rumi, J.L. Shamshina, N. Abidi, Utilization of Cellulose to its Full potential: a Review on Cellulose Dissolution, Regeneration, and applications, Polymers 13 (24) (2021) 4344, https://doi.org/10.3390/polym13244344.

[2] M.R. Ahmed-Haras, N. Kao, L. Ward, M.S. Islam, Insights into the production and Physicochemical Properties of Oxycellulose Microcrystalline with Coexisting Crystalline Forms, Int. J. Biol. Macromol. 146 (March) (2020) 150–161, https://doi.org/10.1016/j.ijbiomac.2019.12.083.

[3] A.K. Alanazi, An innovative Preparation, Characterization, and Optimization of Nanocellulose Fibers (NCF) using Ultrasonic Waves, Polymers 14 (10) (2022) 1930, https://doi.org/10.3390/polym14101930.

[4] J. Alarcón-Espósito, R. Contreras, R.A. Tapia, P.R. Campodónico, "Gutmann's Donor Numbers Correctly Assess the effect of the Solvent on the Kinetics of SNAr Reactions in Ionic Liquids." *Chemistry – a*, European Journal 22 (37) (2016) 13347–13351, https://doi.org/10.1002/chem.201602237.

[5] F. Ali, L. Reinert, J.-M. Levêque, L. Duclaux, F. Muller, S. Saeed, S.S. Shah, Effect of Sonication Conditions: Solvent, Time, Temperature and Reactor Type on the Preparation of Micron Sized Vermiculite Particles, Ultrason. Sonochem. 21 (3) (2014) 1002–1009, https://doi.org/10.1016/j.ultsonch.2013.10.010.

[6] I.K. Al-Khateeb, S. Hussin, Y.M. Alobaidi, Extraction of Cellulose Nano Crystalline from Cotton by Ultrasonic and its Morphological and Structural Characterization, In (2015). https://www.semanticscholar.org/paper/Extraction-of-Cellulose-Nano-Crystalline-from-by-Al-Khateeb-Hussin/6432446957c581ef9155b4d1d69f643d7e58b66b#citing-papers.

[7] T. Aminabhavi, V.B. Patil, Density, Viscosity, Refractive Index, and speed of Sound in Binary Mixtures of Ethenylbenzene with N,N-Dimethylacetamide, Tetrahydrofuran, N,N-Dimethylformamide, 1,4-Dioxane, Dimethyl Sulfoxide, Chloroform, Bromoform, and 1-Chloronaphthalene in the Temperature Interval (298.15−308.15) K, J. Chem. Eng. Data 43 (4) (1998) 497–503, https://doi.org/10.1021/je980031y.

[8] Andrade, Fabia K., João Paulo S. Morais, Celli R. Muniz, José Heriberto O. Nascimento, Rodrigo S. Vieira, Francisco Miguel P. Gama, and Morsyleide F. Rosa. 2019. "Stable Microfluidized Bacterial Cellulose Suspension." *Cellulose* 26 (10): 5851–64. doi:10.1007/s10570-019-02512-y.

[9] P. Arya, A. Srivastava, S.V. Vasaikar, G. Mukherjee, P. Mishra, B. Kundu, Selective Interception of Gelsolin Amyloidogenic Stretch results in Conformationally Distinct Aggregates with Reduced Toxicity, ACS Chem. Nerosci. 5 (10) (2014) 982–992, https://doi.org/10.1021/cn500002v.

[10] B. Baghaei, M. Skrifvars, All-Cellulose Composites: a Review of recent Studies on Structure, Properties and applications, Molecules 25 (12) (2020) 2836, https://doi.org/10.3390/molecules25122836.

[11] A. Berlin, V. Maximenko, R. Bura, K.-Y. Kang, N. Gilkes, J. Saddler, A Rapid Microassay to Evaluate Enzymatic Hydrolysis of Lignocellulosic Substrates, Biotechnol. Bioeng. 93 (5) (2006) 880–886, https://doi.org/10.1002/bit.20783.

[12] Bistac, S., and M. Brogly. 2001. "10.2 EFFECT OF POLYMER/SOLVENT ACID-BASE INTERACTIONS: RELEVANCE TO THE AGGREGATION OF PMMA." In *Handbook of Solvents*, 570–83. ChemTec Publishing - William Andrew, Toronto - New York.

[13] Bistac, S., and J. Schultz. 1997. "Influence of Polymer/Solvent Acid-base Interactions on the Aggregation of Stereoregular PMMA." doi:10.1002/MACP.1997.021980225.

[14] L.S. Blachechen, J. Paulo, E. de Mesquita, L. de Paula, F.V. Pereira, D.F.S. Petri, Interplay of Colloidal Stability of Cellulose Nanocrystals and their Dispersibility in Cellulose Acetate Butyrate Matrix, Cellul. 20 (3) (2013) 1329–1342, https://doi.org/10.1007/s10570-013-9881-y.

[15] Y. Boluk, Acid–Base Interactions and Swelling of Cellulose Fibers in Organic Liquids, Cellul. 12 (6) (2005) 577–593, https://doi.org/10.1007/s10570-005-9004-5.

[16] A. Brinkmann, M. Chen, M. Couillard, Z.J. Jakubek, T. Leng, L.J. Johnston, Correlating Cellulose Nanocrystal Particle size and Surface Area, Langmuir 32 (24) (2016) 6105–6114, https://doi.org/10.1021/acs.langmuir.6b01376.

[17] C. Chacon, W. Daniel, S. Verruck, A.R. Monteiro, G.A. Valencia, The Mechanism, Biopolymers and active Compounds for the production of Nanoparticles by Anti-Solvent Precipitation: a Review, Food Res. Int. 168 (June) (2023) 112728, https://doi.org/10.1016/j.foodres.2023.112728.

[18] P. Calvini, A. Gorassini, G. Luciano, E. Franceschi, FTIR and WAXS Analysis of Periodate Oxycellulose: evidence for a Cluster Mechanism of Oxidation, Vib. Spectrosc 40 (2) (2006) 177–183, https://doi.org/10.1016/j.vibspec.2005.08.004.

[19] C. Cametti, P. Codastefano, R. D'Amato, A. Furlani, M.V. Russo, Static and Dynamic Light Scattering Measurements of Polyphenylacetylene (PPA) in Different Organic Solvents (Tetrahydrofuran, Toluene and Chloroform), Synth. Met. 114 (2) (2000) 173–1119, https://doi.org/10.1016/S0379-6779(00)00245-9.

[20] J.P.F. Carvalho, A.C.Q. Silva, A.J.D. Silvestre, C.S.R. Freire, C. Vilela, Spherical Cellulose Micro and Nanoparticles: a Review of recent Developments and applications, Nanomaterials 11 (10) (2021) 2744, https://doi.org/10.3390/nano11102744.

[22] J.-D. Chai, M. Head-Gordon, Long-Range Corrected Hybrid Density Functionals with Damped Atom–Atom Dispersion Corrections, PCCP 10 (44) (2008) 6615–6620, https://doi.org/10.1039/B810189B.

[23] H. Chang, J. Luo, A.A. Bakhtiary, A.-T. Davijani, H. Po-Hsiang Wang, C. Liu, S. Kumar, Individually Dispersed Wood-based Cellulose Nanocrystals, ACS Appl. Mater. Interfaces 8 (9) (2016) 5768–5771, https://doi.org/10.1021/acsami.6b00094.

[24] Y.-L. Chen, X. Zhang, T.-T. You, Xu. Feng, Deep Eutectic Solvents (DESs) for Cellulose Dissolution: a Mini-Review, Cellul. 26 (1) (2019) 205–213, https://doi.org/10.1007/s10570-018-2130-7.

[25] M. Cheng, Z. Qin, Y. Liu, Y. Qin, T. Li, L. Chen, M. Zhu, Efficient Extraction of Carboxylated Spherical Cellulose Nanocrystals with Narrow distribution through Hydrolysis of Lyocell Fibers by using ammonium Persulfate as an Oxidant, J. Mater. Chem. A 2 (1) (2013) 251–1228, https://doi.org/10.1039/C3TA13653A.

[26] S. Cui, S. Zhang, S. Ge, L. Xiong, Q. Sun, Green Preparation and Characterization of Size-Controlled Nanocrystalline Cellulose via Ultrasonic-Assisted Enzymatic Hydrolysis, Ind. Crop. Prod. 83 (May) (2016) 346–352, https://doi.org/10.1016/j.indcrop.2016.01.019.

[27] B. Dahneke, *Measurement of Suspended Particles by Quasi-Elastic Light Scattering*, Wiley Interscience, New York, 1983.

[28] F. D'Anna, S. Marullo, G. Lazzara, P. Vitale, R. Noto, "aggregation Processes of Perylene Bisimide Diimidazolium Salts" 21 (42) (2015), https://doi.org/10.1002/chem.201502240.

[29] O. Derkacheva, D. Sukhov, Investigation of Lignins by FTIR Spectroscopy, Macromol. Symp. 265 (1) (2008) 61–68, https://doi.org/10.1002/masy.200850507.

[30] D.i. Giorgio, L.M. Luciana, P.R. Salgado, A.N. Mauri, Synthesis and Conservation of Cellulose Nanocrystals, Carbohydr. Polym. 238 (June) (2020) 116187, https://doi.org/10.1016/j.carbpol.2020.116187.

[31] S.E. Domínguez, M. Cangiotti, A. Fattori, T. Ääritalo, P. Damlin, M.F. Ottaviani, C. Kvarnström, Effect of Spacer Length and Solvent on the Concentration-Driven Aggregation of Cationic Hydrogen-Bonding Donor Polythiophenes, Langmuir 34 (25) (2018) 7364–7378, https://doi.org/10.1021/acs.langmuir.8b00808.

[34] S.E. Domínguez, A. Vuolle, A. Fattori, T. Ääritalo, M. Cangiotti, M. Pia Damlin, F. Ottaviani, C. Kvarnström, Enhancement of Charge-Assisted Hydrogen Bond Capabilities due to O-Alkylation Proximity in Alkoxy Cationic Polythiophenes: Solution- and Solid-State evidence via EPR, AFM and Surface Free Energy, PCCP 24 (10) (2022) 6011–6025, https://doi.org/10.1039/D1CP04792B.

[35] Droppo, Ian G. 2006. "Filtration in Particle Size Analysis." In *Encyclopedia of Analytical Chemistry*. American Cancer Society. doi:10.1002/9780470027318.a1506.

[36] A. Dufresne, Nanocellulose: a New Ageless Bionanomaterial, Mater. Today 16 (6) (2013) 220–227, https://doi.org/10.1016/j.mattod.2013.06.004.

[40] E.l. Seoud, A. Omar, M. Kostag, K. Jedvert, N.I. Malek, Cellulose Regeneration and Chemical Recycling: closing the 'Cellulose Gap' using Environmentally Benign Solvents, Macromol. Mater. Eng. 305 (4) (2020) 1900832, https://doi.org/10.1002/mame.201900832.

[41] A. Errokh, A. Magnin, J.-L. Putaux, S. Boufi, Morphology of the Nanocellulose Produced by Periodate Oxidation and Reductive Treatment of Cellulose Fibers, Cellul. 25 (7) (2018) 3899–3911, https://doi.org/10.1007/s10570-018-1871-7.

[42] Z. Fan, J. Chen, W. Guo, F. Ma, S. Sun, Q. Zhou, Crystallinity of Regenerated Cellulose from [Bmim]Cl Dependent on the Hydrogen Bond Acidity/Basicity of Anti-Solvents, RSC Adv. 7 (65) (2017) 41004–41010, https://doi.org/10.1039/C7RA08178B.

[43] Z. Fan, J. Chen, W. Guo, F. Ma, S. Sun, Q. Zhou, Anti-Solvents Tuning Cellulose Nanoparticles through two Competitive Regeneration Routes, Cellul. 25 (8) (2018) 4513–4523, https://doi.org/10.1007/s10570-018-1897-x.

[44] W. Focke, C.E. Weikowitsch, Untersuchungen über Zusammenhänge Zwischen Einigen Mikroskopischen Und Makroskopischen Eigenschaften Flüssiger Organischer Systeme, Zeitschrift Für Physikalische Chemie 111 (2) (1978) 153–162, https://doi.org/10.1524/zpch.1978.111.2.153.

[45] J.-F. Gal, P.-C. Maria, Can the Lewis Basicity of an Isolated Solvent Molecule Be used for Characterizing Solvent Effects? Curr. Anal. Chem. 17 (3) (2021) 328–338.
[46] Gargallo, L., and D. Radic. 2001. "5.4 MIXED SOLVENTS, A WAY TO CHANGE THE POLYMER SOLUBILITY." In *Handbook of Solvents*, 267–80. ChemTec Publishing - William Andrew, Toronto - New York.
[48] Y. Grohens, G. Castelein, P. Carriere, J. Spevacek, J. Schultz, Multiscale Aggregation of PMMA Stereocomplexes at a Surface: an Atomic Force Microscopy Investigation, Langmuir 17 (1) (2001) 86–94, https://doi.org/10.1021/la000879w.
[49] Hansen, Charles M. 2007. *Hansen Solubility Parameters: A User's Handbook, Second Edition*. 2nd ed. Boca Raton: CRC Press. doi:10.1201/9781420006834.
[50] M.D. Hanwell, D.E. Curtis, D.C. Lonie, T. Vandermeerschd, E. Zurek, G. R. Hutchison, Avogadro: an Advanced Semantic Chemical Editor, Visualization, and Analysis Platform, J. Cheminf. 4 (8) (2012) 1–17, https://doi.org/10.1186/1758-2946-4-17.
[51] G.A. Haron, H.M. Suliman, H.B. Noh, M. Goto, M. Moniruzzaman, Cellulose Nanocrystals Preparation from Microcrystalline Cellulose using Ionic Liquid-DMSO Binary Mixture as a Processing Medium, J. Mol. Liq. 346 (January) (2022) 118208, https://doi.org/10.1016/j.molliq.2021.118208.
[52] L.K.J. Hauru, M. Hummel, A.W.T. King, I. Kilpeläinen, H. Sixta, Role of Solvent Parameters in the Regeneration of Cellulose from Ionic Liquid Solutions, Biomacromolecules 13 (9) (2012) 2896–2905, https://doi.org/10.1021/bm300912y.
[53] S. Hedjazi, S.H. Razavi, A Comparison of Canthaxanthine Pickering Emulsions, Stabilized with Cellulose Nanocrystals of Different Origins, Int. J. Biol. Macromol. 106 (January) (2018) 489–497, https://doi.org/10.1016/j.ijbiomac.2017.08.030.
[54] T. Heinze, A. Koschella, Solvents Applied in the Field of Cellulose Chemistry: a Mini Review, Polímeros 15 (June) (2005) 84–90, https://doi.org/10.1590/S0104-14282005000200005.
[55] D.Y. Hoo, Z.L. Low, D.Y.S. Low, S.Y. Tang, S. Manickam, K.W. Tan, Z.H. Ban, Ultrasonic Cavitation: an Effective Cleaner and Greener Intensification Technology in the Extraction and Surface Modification of Nanocellulose, Ultrason. Sonochem. 90 (November) (2022) 106176, https://doi.org/10.1016/j.ultsonch.2022.106176.
[57] Y. Hu, N. Abidi, Distinct Chiral Nematic Self-Assembling Behavior Caused by Different Size-Unified Cellulose Nanocrystals via a Multistage Separation, Langmuir 32 (38) (2016) 9863–9872, https://doi.org/10.1021/acs.langmuir.6b02861.
[58] Yu. Huang, L. Wang, Y. Chao, D.S. Nawawi, T. Akiyama, T. Yokoyama, Y. Matsumoto, Analysis of Lignin Aromatic Structure in Wood based on the IR Spectrum, J. Wood Chem. Technol. 32 (4) (2012) 294–303, https://doi.org/10.1080/02773813.2012.666316.
[59] W. Humphrey, A. Dalke, K. Schulten, VMD: Visual Molecular Dynamics, J. Mol. Graph. 14 (1) (1996) 33–38, https://doi.org/10.1016/0263-7855(96)00018-5.
[61] Islam, Tariqul, Md Zaidul Islam Sarker, ABM Helal Uddin, Kamaruzzaman Bin Yunus, Reddy Prasad D.M, Md Abdur Rashid Mia, and Sahena Ferdosh. 2020. "Kamlet Taft Parameters: A Tool to Alternate the Usage of Hazardous Solvent in Pharmaceutical and Chemical Manufacturing/Synthesis - A Gateway towards Green Technology." *Analytical Chemistry Letters*, September. https://www.tandfonline.com/doi/abs/10.1080/22297928.2020.1860124.
[62] Z.J. Jakubek, M. Chen, M. Couillard, T. Leng, L. Liu, S. Zou, U. Baxa, J. D. Clogston, W.Y. Hamad, L.J. Johnston, Characterization challenges for a Cellulose Nanocrystal Reference Material: Dispersion and Particle size Distributions, J. Nanopart. Res. 20 (4) (2018) 98, https://doi.org/10.1007/s11051-018-4194-6.
[64] Johnson, C. S. Jr., and D. A. Gabriel. 1981. *Laser Light Scattering*. New York: Dover Publications Inc.
[65] J.H. Jordan, M.W. Easson, B.D. Condon, Cellulose Hydrolysis using Ionic Liquids and Inorganic Acids under Dilute Conditions: Morphological Comparison of Nanocellulose, RSC Adv. 10 (65) (2020) 39413–39424, https://doi.org/10.1039/D0RA05976E.
[66] H. Jørgensen, J.B. Kristensen, C. Felby, Enzymatic Conversion of Lignocellulose into Fermentable Sugars: challenges and Opportunities, Biofuels Bioprod. Biorefin. 1 (2) (2007) 119–134, https://doi.org/10.1002/bbb.4.
[67] M. Jurak, K. Szafran, P. Cea, S. Martín, Analysis of Molecular Interactions between Components in Phospholipid-Immunosuppressant-Antioxidant mixed Langmuir Films, Langmuir 37 (18) (2021) 5601–5616, https://doi.org/10.1021/acs.langmuir.1c00434.
[69] Z. Kan, Q. Zhu, L. Yang, Z. Huang, B. Jin, J. Ma, Polarization Effects on the Cellulose Dissolution in Ionic Liquids: Molecular Dynamics Simulations with Polarization Model and Integrated Tempering Enhanced Sampling Method, J. Phys. Chem. B 121 (17) (2017) 4319–4332, https://doi.org/10.1021/acs.jpcb.6b12647.
[70] S.G. Khokarale, P. Jablonski, D. Nikjoo, V.M. Dinh, O. Sundman, K. Irgum, J.-P. Mikkola, Poly (Vinylidene Difluoride) Polymer in 1-Ethyl-3-Methylimidazolium Acetate and Acetic Acid Containing Solvents: Tunable and Recoverable Solvent Media to Induce Crystalline phase transition and Porosity, Sustainable Chemistry 3 (4) (2022) 455–474, https://doi.org/10.3390/suschem3040028.
[71] G.S. Komal, G. Singh, T.S. Kang, Aggregation Behavior of Sodium Dioctyl Sulfosuccinate in Deep Eutectic Solvents and their Mixtures with Water: an Account of Solvent's Polarity, Cohesiveness, and Solvent Structure, ACS Omega, October. (2018), https://doi.org/10.1021/acsomega.8b01637.
[72] E. Kontturi, T. Tammelin, M. Österberg, Cellulose—Model Films and the Fundamental Approach, Chem. Soc. Rev. 35 (12) (2006) 1287–1304, https://doi.org/10.1039/B601872F.
[73] G. Krawczyk, A. Venables, F.M.C. Tuason, Chapter 27 - Microcrystalline Cellulose, in: G.O. Phillips, P.A. Williams (Eds.), *Handbook of Hydrocolloids (second Edition)*, Woodhead Publishing, 2009, pp. 740–1459.
[74] A. Larsson, W.E. Johns, Acid-Base Interactions between Cellulose/Lignocellulose and Organic Molecules, J. Adhes. 25 (2) (1988) 121–131, https://doi.org/10.1080/00218468808071254.
[75] Q. Li, S. Renneckar, Supramolecular Structure Characterization of Molecularly Thin Cellulose I Nanoparticles, Biomacromolecules 12 (3) (2011) 650–669, https://doi.org/10.1021/bm101315y.
[77] Liebert, Tim. 2010. "Cellulose Solvents – Remarkable History, Bright Future." In *Cellulose Solvents: For Analysis, Shaping and Chemical Modification*, 1033:3–54. ACS Symposium Series 1033. American Chemical Society. doi:10.1021/bk-2010-1033.ch001.
[78] Y.H. Lim, I.M.L. Chew, T.S.Y. Choong, M.C. Tan, K.W. Tan, NanoCrystalline Cellulose Isolated from Oil Palm empty Fruit Bunch and its potential in Cadmium Metal Removal, MATEC Web of Conferences 59 (2016) 04002, https://doi.org/10.1051/matecconf/20165904002.
[79] B. Lindman, B. Medronho, L. Alves, C. Costa, H. Edlund, M. Norgren, The Relevance of Structural Features of Cellulose and its Interactions to Dissolution, Regeneration, Gelation and Plasticization Phenomena, PCCP 19 (35) (2017) 23704–23718, https://doi.org/10.1039/C7CP02409F.
[80] R. López-Simeon, J. Campos-Terán, H.I. Beltrán, M. Hernández-Guerrero, Free-Lignin Cellulose Obtained from Agar Industry Residues using a Continuous and Minimal Solvent Reaction/Extraction Methodology, RSC Adv. 2 (32) (2012) 12286–12297, https://doi.org/10.1039/C2RA22185C.
[81] T. Lu, F. Chen, Multiwfn: a Multifunctional Wavefunction Analyzer, J. Comput. Chem. 33 (5) (2012) 580–592, https://doi.org/10.1002/jcc.22885.
[82] X. Lu, Xu. Shujun, J. Chen, L. Ni, X. Ma, S. Cao, H. Gao, Cellulose Dissolution in Ionic Liquid from Hydrogen Bonding Perspective: First-Principles Calculations, Cellul. 30 (7) (2023) 4181–4195, https://doi.org/10.1007/s10570-023-05140-9.
[83] J. Lyklema, Langmuir Monolayers, in: Fundamentals of Interface and Colloid Science, 3, Elsevier, 2000, https://doi.org/10.1016/S1874-5679(00)80006-9.
[85] M. Mattonai, D. Pawcenis, S. del Seppia, J. Łojewska, E. Ribechini, Effect of Ball-Milling on Crystallinity Index, Degree of Polymerization and thermal Stability of Cellulose, Bioresour. Technol. 270 (December) (2018) 270–327, https://doi.org/10.1016/j.biortech.2018.09.029.
[86] B. Mazela, W. Perdoch, B. Peplińska, M. Zieliński, Influence of Chemical Pre-Treatments and Ultrasonication on the Dimensions and Appearance of Cellulose Fibers, Materials 13 (22) (2020) 5274, https://doi.org/10.3390/ma13225274.
[87] C. McDowell, M. Abdelsamie, M.F. Toney, G.C. Bazan, Solvent Additives: Key Morphology-Directing Agents for Solution-Processed Organic Solar Cells, Adv. Mater. 30 (33) (2018), https://doi.org/10.1002/adma.201707114.
[89] B. Medronho, B. Lindman, Competing forces during Cellulose Dissolution: from Solvents to Mechanisms, Curr. Opin. Colloid Interface Sci. 19 (1) (2014) 32–40, https://doi.org/10.1016/j.cocis.2013.12.001.
[90] Michelsen, Peter. 1990. "Relationship between Chromatographic Retention and Donor and Acceptor Numbers." *Theses*, December. https://repository.rit.edu/theses/6013.
[92] S. Mittal, S. Prasad, R.S. Payal, S. Ravi, Ab-Initio Study on the Covalent Nature of Hydrogen Bonding in Cellobiose, Cellul. 30 (2) (2023) 689–704, https://doi.org/10.1007/s10570-022-04939-2.
[94] B. Morgenstern, H.-W. Kammer, On the Particulate Structure of Cellulose Solutions, Polymer 40 (5) (1999) 1299–1304, https://doi.org/10.1016/S0032-3861(98)00267-5.
[95] H.-Y. Mou, E. Orblin, K. Kruus, P. Fardim, Topochemical Pretreatment of Wood Biomass to Enhance Enzymatic Hydrolysis of Polysaccharides to Sugars, Bioresour. Technol. 142 (August) (2013) 540–555, https://doi.org/10.1016/j.biortech.2013.05.046.
[97] K. Noworyta, P. Kuran, E.A. Nantsis, R. Bilewicz, L. Dunsch, W. Kutner, Surface Properties of Langmuir Films of Mono-, Di-, and Tetra-*n*-Octyl Adducts of C60 at the Water–Air Interface, Synth. Met. 123 (1) (2001) 157–164, https://doi.org/10.1016/S0379-6779(00)01323-0.
[98] S.Y. Oh, D.I. Yoo, Y. Shin, G. Seo, FTIR Analysis of Cellulose Treated with Sodium Hydroxide and Carbon Dioxide, Carbohydr. Res. 340 (3) (2005) 417–428, https://doi.org/10.1016/j.carres.2004.11.027.
[99] H. Okura, M. Wada, T. Serizawa, Dispersibility of HCl-Treated Cellulose Nanocrystals with Water-Dispersible Properties in Organic Solvents, Chem. Lett. 43 (5) (2014) 601–603, https://doi.org/10.1246/cl.131181.
[101] N. Pandi, S.H. Sonawane, K. Anand Kishore, Synthesis of Cellulose Nanocrystals (CNCs) from Cotton using Ultrasound-Assisted Acid Hydrolysis, Ultrason. Sonochem. 70 (January) (2021) 105353, https://doi.org/10.1016/j.ultsonch.2020.105353.
[102] Z. Pang, P. Wang, C. Dong, Ultrasonic Pretreatment of Cellulose in Ionic Liquid for Efficient Preparation of Cellulose Nanocrystals, Cellul. 25 (12) (2018) 7053–7064, https://doi.org/10.1007/s10570-018-2070-2.
[103] Papadakis, Raffaello, Ioanna Deligkiozi, Raffaello Papadakis, and Ioanna Deligkiozi. 2019. "Solvent Effects in Supramolecular Systems." In *Solvents, Ionic Liquids and Solvent Effects*. IntechOpen. doi:10.5772/intechopen.86981.
[104] S. Park, J.O. Baker, M.E. Himmel, P.A. Parilla, D.K. Johnson, Cellulose Crystallinity Index: Measurement Techniques and their Impact on Interpreting Cellulase Performance, Biotechnol. Biofuels 3 (1) (2010) 10, https://doi.org/10.1186/1754-6834-3-10.

[105] M.K. Patoary, A. Farooq, F. Yinan, A. Chaudary, S.R. Islam, Y. Zhao, A. Ge, F. Wang, L. Liu, Structure and Rheological Studies of Phosphorylated Cellulose Nanofibrils Suspensions, Ind. Crop. Prod. 178 (April) (2022) 114581, https://doi.org/10.1016/j.indcrop.2022.114581.
[106] P. Thoresen, H.L. Petter, U. Rova, P. Christakopoulos, L. Matsakas, Role and Importance of Solvents for the Fractionation of Lignocellulosic Biomass, Bioresour. Technol. 369 (February) (2023) 128447, https://doi.org/10.1016/j.biortech.2022.128447.
[107] P. Paximada, E.A. Dimitrakopoulou, E. Tsouko, A.A. Koutinas, C. Fasseas, I. G. Mandala, Structural Modification of Bacterial Cellulose Fibrils under Ultrasonic Irradiation, Carbohydr. Polym. 150 (October) (2016) 5–12, https://doi.org/10.1016/j.carbpol.2016.04.125.
[108] R. Pecora, *Dynamic Light Scattering: applications of Photon Correlation Spectroscopy*, Plenum Press, 1985.
[109] M. Peesan, A. Sirivat, P. Supaphol, R. Rujiravanit, Dilute solution Properties of Hexanoyl Chitosan in Chloroform, Dichloromethane, and Tetrahydrofuran, Carbohydr. Polym. 64 (2) (2006) 175–183, https://doi.org/10.1016/j.carbpol.2005.11.010.
[110] M. Reimer, F. Eckel, M. Rothammer, D. Van Opdenbosch, C. Zollfrank, Manufacturing of Cellulose-based Nano- and Submicronparticles via Different Precipitation Methods, Cellul. 30 (14) (2023) 8861–8881, https://doi.org/10.1007/s10570-023-05397-0.
[112] R.J. Rubira, P.H. Gonçalves, B. Aoki, C.J.L. Constantino, P. Alessio, Supramolecular Architectures of Iron Phthalocyanine Langmuir-Blodgett Films: the Role Played by the solution Solvents, Appl. Surf. Sci. 416 (September) (2017) 482–491, https://doi.org/10.1016/j.apsusc.2017.04.155.
[113] K.S. Salem, N.K. Kasera, M.A. Rahman, H. Jameel, Y. Habibi, S.J. Eichhorn, A. D. French, L. Pal, L.A. Lucia, Comparison and Assessment of Methods for Cellulose Crystallinity Determination, Chem. Soc. Rev. 52 (18) (2023) 6417–6446, https://doi.org/10.1039/D2CS00569G.
[115] M. Schmeisser, P. Illner, R. Puchta, A. Zahl, R. van Eldik, "Gutmann Donor and Acceptor Numbers for Ionic Liquids." *Chemistry – a*, European Journal 18 (35) (2012) 10969–10982, https://doi.org/10.1002/chem.201200584.
[116] T.I. Shaheen, H.E. Emam, Sono-Chemical Synthesis of Cellulose Nanocrystals from Wood Sawdust using Acid Hydrolysis, Int. J. Biol. Macromol. 107 (February) (2018) 1599–1606, https://doi.org/10.1016/j.ijbiomac.2017.10.028.
[117] A.A. Shamsuri, K. Abdan, S.N.A.M. Jamil, Properties and applications of Cellulose Regenerated from Cellulose/Imidazolium-based Ionic Liquid/Co-Solvent Solutions: a Short Review, E-Polymers 21 (1) (2021) 869–880, https://doi.org/10.1515/epoly-2021-0086.
[118] E. Sharifzadeh, M. Karami, F. Ader, Formation of Nanoparticle Aggregates and Agglomerates in Polymer Nanocomposites and their Distinct Impacts on the Mechanical Properties, Polym. Eng. Sci. 63 (4) (2023) 1303–1313, https://doi.org/10.1002/pen.26284.
[120] G. Siqueira, A.MF. Milagres, W. Carvalho, G. Koch, A. Ferraz, Topochemical distribution of Lignin and Hydroxycinnamic Acids in Sugar-Cane Cell Walls and its Correlation with the Enzymatic Hydrolysis of Polysaccharides, Biotechnol. Biofuels 4 (1) (2011) 7, https://doi.org/10.1186/1754-6834-4-7.
[121] M.R. Sofla, R.J. Kord, T.T. Brown, T.J. Rainey, A Comparison of Cellulose Nanocrystals and Cellulose Nanofibres Extracted from Bagasse using Acid and Ball Milling Methods, Adv. Nat. Sci. Nanosci. Nanotechnol. 7 (3) (2016) 035004, https://doi.org/10.1088/2043-6262/7/3/035004.
[123] G. SriBala, R. Chennuru, S. Mahapatra, R. Vinu, Effect of Alkaline Ultrasonic Pretreatment on Crystalline Morphology and Enzymatic Hydrolysis of Cellulose, Cellul. 23 (3) (2016) 1725–1740, https://doi.org/10.1007/s10570-016-0893-2.
[124] S. Sumari, A. Roesyadi, S. Sumarno, Effects of Ultrasound on the Morphology, Particle size, Crystallinity, and Crystallite size of Cellulose, Scientific Study & Research Chemistry & Chemical Engineering, Biotechnology, Food Industry 14 (4) (2013) 229–239.
[125] A. Taheri, M. Mohammadi, The use of Cellulose Nanocrystals for potential Application in Topical delivery of Hydroquinone, Chem. Biol. Drug Des. 86 (1) (2015) 102–106, https://doi.org/10.1111/cbdd.12466.
[126] H. Takagi, T. Isoda, K. Kusakabe, S. Morooka, Effects of Solvents on the Hydrogenation of Mono-Aromatic Compounds using Noble-Metal Catalysts, Energy Fuel 13 (6) (1999) 1191–2116, https://doi.org/10.1021/ef990061m.
[127] Teles, Ana Rita R., Emanuel V. Capela, Rafael S. Carmo, João A.P. Coutinho, Armando J.D. Silvestre, and Mara G. Freire. 2017. "Solvatochromic Parameters of Deep Eutectic Solvents Formed by Ammonium-Based Salts and Carboxylic Acids." *Fluid Phase Equilibria* 448 (September):15–21. doi:10.1016/j.fluid.2017.04.020.
[129] A.A. Thorat, S.V. Dalvi, Liquid Antisolvent Precipitation and Stabilization of Nanoparticles of Poorly Water Soluble Drugs in Aqueous Suspensions: recent Developments and Future Perspective, Chem. Eng. J. 181–182 (February) (2012) 1–34, https://doi.org/10.1016/j.cej.2011.12.044.
[130] Y. Tomimatsu, H. Suetsugu, Y. Yoshimura, A. Shimizu, The Solubility of Cellulose in Binary Mixtures of Ionic Liquids and Dimethyl Sulfoxide: Influence of the Anion, J. Mol. Liq. 279 (April) (2019) 120–216, https://doi.org/10.1016/j.molliq.2019.01.093.
[131] N. Trišović, N. Valentić, M. Erović, T. Đaković-Sekulić, G. Uščumlić, I. Juranić, Synthesis, Structure, and Solvatochromic Properties of Pharmacologically active 5-Substituted 5-Phenylhydantoins, Monatshefte Für Chemie - Chemical Monthly 142 (12) (2011) 1227–1234, https://doi.org/10.1007/s00706-011-0639-7.
[132] M. Uhlig, A. Fall, S. Wellert, M. Lehmann, S. Prévost, L. Wågberg, R. von Klitzing, G. Nyström, Two-Dimensional Aggregation and Semidilute Ordering in Cellulose Nanocrystals, Langmuir 32 (2) (2016) 442–450, https://doi.org/10.1021/acs.langmuir.5b04008.
[133] S. Ventura-Cruz, A. Tecante, Nanocellulose and Microcrystalline Cellulose from Agricultural Waste: Review on Isolation and Application as Reinforcement in Polymeric Matrices, Food Hydrocoll. 118 (September) (2021) 106771, https://doi.org/10.1016/j.foodhyd.2021.106771.
[134] Verma, Chandrabhan, Ankush Mishra, Swati Chauhan, Pratibha Verma, Vandana Srivastava, M. A. Quraishi, and Eno E. Ebenso. 2019. "Dissolution of Cellulose in Ionic Liquids and Their Mixed Cosolvents: A Review." *Sustainable Chemistry and Pharmacy* 13 (September):100162. doi:10.1016/j.scp.2019.100162.
[135] C. Verma, M. Chhajed, P. Gupta, S. Roy, P.K. Maji, Isolation of Cellulose Nanocrystals from Different Waste Bio-Mass Collating their Liquid Crystal Ordering with Morphological Exploration, Int. J. Biol. Macromol. 175 (April) (2021) 242–253, https://doi.org/10.1016/j.ijbiomac.2021.02.038.
[137] M.I. Voronova, O.V. Surov, N.V. Rubleva, N.E. Kochkina, A.G. Zakharov, Dispersibility of Nanocrystalline Cellulose in Organic Solvents, Russ. J. Bioorg. Chem. 46 (7) (2020) 1295–1303, https://doi.org/10.1134/S106816202007016X.
[139] H. Wang, G. Gurau, R.D. Rogers, Ionic Liquid Processing of Cellulose, Chem. Soc. Rev. 41 (4) (2012) 1519–1537, https://doi.org/10.1039/C2CS15311D.
[140] Y. Wang, Q. Wang, Y. Zhu, Y. Shen, S. Cheng, H. Zheng, Xu. Yunhui, Structure and Properties of Oxycellulose fabric Crosslinked with Soy Protein, Carbohydr. Polym. 257 (April) (2021) 117548, https://doi.org/10.1016/j.carbpol.2020.117548.
[141] E.Y. Wardhono, N. Kanani, A. Alfirano, A simple Process of Isolation Microcrystalline Cellulose using Ultrasonic Irradiation, J. Dispers. Sci. Technol. 41 (8) (2020) 1217–1226, https://doi.org/10.1080/01932691.2019.1614947.
[142] Washington, Clive. 1992. *Particle Size Analysis In Pharmaceutics And Other Industries: Theory And Practice: Theory And Practice*. London: CRC Press. doi:10.1201/b12596.
[143] C. Wu, D.J. McClements, M. He, L.i. Zheng, T. Tian, F. Teng, Y. Li, Preparation and Characterization of Okara Nanocellulose Fabricated using Sonication or High-pressure Homogenization Treatments, Carbohydr. Polym. 255 (March) (2021) 117364, https://doi.org/10.1016/j.carbpol.2020.117364.
[144] Y. Xu, A.D. Atrens, J.R. Stokes, Rheology and Microstructure of Aqueous Suspensions of Nanocrystalline Cellulose Rods, J. Colloid Interface Sci. 496 (June) (2017) 130–140, https://doi.org/10.1016/j.jcis.2017.02.020.
[145] C. Yadav, A. Saini, P.K. Maji, Energy Efficient Facile Extraction Process of Cellulose Nanofibres and their Dimensional Characterization using Light Scattering Techniques, Carbohydr. Polym. 165 (June) (2017) 276–284, https://doi.org/10.1016/j.carbpol.2017.02.049.
[146] H. Yang, R. Yan, H. Chen, D.H. Lee, C. Zheng, Characteristics of Hemicellulose, Cellulose and Lignin Pyrolysis, Fuel 86 (12) (2007) 1781–2178, https://doi.org/10.1016/j.fuel.2006.12.013.
[147] Yaw, Carl L. 2008. *Thermophysical Properties of Chemicals and Hydrocarbons*. 1st ed. Norwich, NY: William Andrew.
[148] B. Zakani, D. Grecov, Effect of Ultrasonic Treatment on Yield stress of Highly Concentrated Cellulose Nano-Crystalline (CNC) Aqueous Suspensions, Carbohydr. Polym. 291 (September) (2022) 119651, https://doi.org/10.1016/j.carbpol.2022.119651.
[149] H. Zhang, L. González-Aguilera, M. Daniel López, L. Ferrer, F. del Monte, M. C. Gutiérrez, Hydrogen Bonding in Ternary Mixtures of N-Methyl Morpholine Oxide, Water and Dimethyl Sulfoxide for Enhanced Cellulose Dissolution Capabilities, J. Mol. Liq. 358 (July) (2022) 119113, https://doi.org/10.1016/j.molliq.2022.119113.
[150] L. Zhang, C. Huang, C. Zhang, H. Pan, Swelling and Dissolution of Cellulose in Binary Systems of Three Ionic Liquids and Three Co-Solvents, Cellul. 28 (8) (2021) 4643–4653, https://doi.org/10.1007/s10570-021-03844-4.
[151] L. Zhang, Yu. Haitao, S. Liu, Y. Wang, Mu. Tiancheng, Z. Xue, Kamlet–Taft Parameters of Deep Eutectic Solvents and their Relationship with Dissolution of Main Lignocellulosic Components, Ind. Eng. Chem. Res. 62 (29) (2023) 11723–11734, https://doi.org/10.1021/acs.iecr.3c01309.
[152] M.-F. Zhang, Y.-H. Qin, J.-Y. Ma, L.i. Yang, Wu. Zai-Kun, T.-L. Wang, W.-G. Wang, C.-W. Wang, Depolymerization of Microcrystalline Cellulose by the Combination of Ultrasound and Fenton Reagent, Ultrason. Sonochem. 31 (July) (2016) 404–408, https://doi.org/10.1016/j.ultsonch.2016.01.027.
[153] Zhong, Fang, and John Nsor-Atindana. 2021. "Chapter 16 - Microcrystalline Cellulose and Nanocrystalline Cellulose." In *Handbook of Hydrocolloids (Third Edition)*, edited by Glyn O. Phillips and Peter A. Williams, 509–36. Woodhead Publishing Series in Food Science, Technology and Nutrition. Woodhead Publishing. doi:10.1016/B978-0-12-820104-6.00021-8.
[154] L.T. Zhuravlev, Concentration of Hydroxyl groups on the Surface of Amorphous Silicas, Langmuir 3 (3) (1987) 316–338, https://doi.org/10.1021/la00075a004.
[155] D.V. Zlenko, D.N. Vtyurina, S.V. Usachev, A.A. Skoblin, M.G. Mikhaleva, G. G. Politenkova, S.N. Nikolsky, S.V. Stovbun, On the Orientation of the Chains in the Mercerized Cellulose, Sci. Rep. 11 (1) (2021) 8765, https://doi.org/10.1038/s41598-021-88040-x.

Further reading

[21] "Cellulose microcrystalline, powder, 20um 9004-34-6." n.d. Accessed December 12, 2022. https://www.sigmaaldrich.com/MX/es/product/aldrich/310697.
[32] S.E. Domínguez, B. Kohn, T. Ääritalo, P. Damlin, U. Scheler, C. Kvarnström, Cationic Polythiophene-Anionic Fullerene Pair in Water and Water-Dioxane: Studies on Hydrogen Bonding Capabilities, Kinetic and Thermodynamic Properties, PCCP 23 (August) (2021) 21013–21028, https://doi.org/10.1039/D0CP05748G, Just accepted.
[33] S.E. Domínguez, A. Vuolle, C. Butler-Hallissey, T. Ääritalo, P. Damlin, C. Kvarnström, J-like Aggregation of a Cationic Polythiophene with Hydrogen-

Bonding Capabilities due to 1,4-Dioxane: solution Excitation Spectra and Fluorescence, Morphology and Surface Free Energy of Films, J. Colloid Interface Sci. 584 (2021) 281–294, https://doi.org/10.1016/j.jcis.2020.09.124.

[37] "Dynamic Light Scattering : An Introduction in 30 Minutes." 2014. 2014. https://www.semanticscholar.org/paper/Dynamic-Light-Scattering-%3A-An-Introduction-in-30/1d28101f3c0b2c4bbcb305f930fdc658f800fac5.

[38] E.l. Seoud, A. Omar, T.A. Bioni, M.T. Dignani, Understanding Cellulose Dissolution in Ionic Liquid-Dimethyl Sulfoxide Binary Mixtures: Quantification of the Relative Importance of Hydrogen Bonding and Hydrophobic Interactions, J. Mol. Liq. 322 (January) (2021) 114848, https://doi.org/10.1016/j.molliq.2020.114848.

[39] E.l. Seoud, A. Omar, M. Kostag, K. Jedvert, N.I. Malek, Cellulose in Ionic Liquids and Alkaline Solutions: advances in the Mechanisms of Biopolymer Dissolution and Regeneration, Polymers 11 (12) (2019) 1917, https://doi.org/10.3390/polym11121917.

[47] "Gaussian 09, Revision A.1 , Gaussian, Inc. Gaussian 09, Revision A.02, M. J. Frisch, G. W. Trucks, H. B. Schlegel, G. E. Scuseria, M. A. Robb, J. R. Cheeseman, G. Scalmani, V. Barone, G. A. Petersson, H. Nakatsuji, X. Li, M. Caricato, A. Marenich, J. Bloino, B. G. Janesko, R. Gomperts, B. Mennucci, H. P. Hratchian, J. V. Ortiz, A. F. Izmaylov, J. L. Sonnenberg, D. Williams-Young, F. Ding, F. Lipparini, F. Egidi, J. Goings, B. Peng, A. Petrone, T. Henderson, D. Ranasinghe, V. G. Zakrzewski, J. Gao, N. Rega, G. Zheng, W. Liang, M. Hada, M. Ehara, K. Toyota, R. Fukuda, J. Hasegawa, M. Ishida, T. Nakajima, Y. Honda, O. Kitao, H. Nakai, T. Vreven, K. Throssell, J. A. Montgomery, Jr., J. E. Peralta, F. Ogliaro, M. Bearpark, J. J. Heyd, E. Brothers, K. N. Kudin, V. N. Staroverov, T. Keith, R. Kobayashi, J. Normand, K. Raghavachari, A. Rendell, J. C. Burant, S. S. Iyengar, J. Tomasi, M. Cossi, J. M. Millam, M. Klene, C. Adamo, R. Cammi, J. W. Ochterski, R. L. Martin, K. Morokuma, O. Farkas, J. B. Foresman, and D. J. Fox, Gaussian, Inc., Wallingford CT, 2016." 2009.

[56] X. Hu, H. Douglas Goff, Fractionation of Polysaccharides by Gradient Non-Solvent Precipitation: a Review, Trends Food Sci. Technol. 81 (November) (2018) 108–115, https://doi.org/10.1016/j.tifs.2018.09.011.

[60] Indarti, Eti, Marwan, and Wanrosli Wan Daud. 2020. "Dispersion Stability of Nanocellulose in Nonpolar Solvent: Chloroform." *Materials Science Forum* 998: 170–75. doi:10.4028/www.scientific.net/MSF.998.170.

[63] "Jmol: An Open-Source Java Viewer for Chemical Structures in 3D. Http://Www.Jmol.Org/." n.d.

[68] Kalász, Huba, Mária Báthori, and Klára L. Valkó. 2020. "Chapter 10 - Basis and Pharmaceutical Applications of Thin-Layer Chromatography." In *Handbook of Analytical Separations*, edited by Klára l. Valkó, 8:523–85. Separation Methods in Drug Synthesis and Purification. Elsevier Science B.V. doi:10.1016/B978-0-444-64070-3.00010-2.

[76] X. Liang, Y. Zhu, B. Qi, S. Li, J. Luo, Y. Wan, Structure-Property-Performance Relationships of Lactic Acid-based Deep Eutectic Solvents with Different Hydrogen Bond Acceptors for Corn Stover Pretreatment, Bioresour. Technol. 336 (September) (2021) 125312, https://doi.org/10.1016/j.biortech.2021.125312.

[84] M. Mariano, N. El Kissi, A. Dufresne, Cellulose Nanocrystals and Related Nanocomposites: Review of some Properties and challenges, J Polym Sci B 52 (12) (2014) 791–806, https://doi.org/10.1002/polb.23490.

[88] Md. Salim, J.A. Rafidah, M.S. Sarjadi, Chemical Functional groups of Extractives, Cellulose and Lignin Extracted from Native Leucaena Leucocephala Bark, Wood Sci. Technol. 55 (2) (2021) 295–313, https://doi.org/10.1007/s00226-020-01258-2.

[91] "MicroCrystalline Cellulose Chemical Characterization Services." n.d. *Excipia* (blog). Accessed December 14, 2022. https://www.excipia.eu/excipients/cellulose-derivatives/microcrystalline-cellulose/.

[93] A. Montes, C. Pereyra, E.J. Martinez de la Ossa, Screening Design of Experiment Applied to the Supercritical Antisolvent Precipitation of Quercetin, J. Supercrit. Fluids 104 (September) (2015) 10–18, https://doi.org/10.1016/j.supflu.2015.05.019.

[96] Nascimento, José Heriberto O. do, Rodrigo F. Luz, Felipe M. F. Galvão, José Daniel D. Melo, Fernando R. Oliveira, Rasiah Ladchumananandasivam, and Andrea Zille. 2015. "Extraction and Characterization of Cellulosic Nanowhisker Obtained from Discarded Cotton Fibers." *Materials Today: Proceedings*, ANM2014: 5th International conference on Advanced Nanomaterials, 2 (1): 1–7. doi:10.1016/j.matpr.2015.04.001.

[100] T.F. O'Mahony, M.A. Morris, Hydroxylation Methods for Mesoporous Silica and their Impact on Surface Functionalisation, Microporous Mesoporous Mater. 317 (April) (2021) 110989, https://doi.org/10.1016/j.micromeso.2021.110989.

[111] Riddle, Floyd L., and Frederick M. Fowkes. 1990. "Spectral Shifts in Acid-Base Chemistry. 1. van Der Waals Contributions to Acceptor Numbers." *J. Am. Chem. Soc.*, 1990. World. doi:10.1021/ja00165a001.

[114] D.T. Sawyer, L. Roberts, *Experimental Electrochemistry for Chemists*, Verlag John Wiley & Sons Ltd., Baffins Lane, 1974.

[119] Shi, Jiangtao, Dong Xing, and Jian Lia. 2012. "FTIR Studies of the Changes in Wood Chemistry from Wood Forming Tissue under Inclined Treatment." *Energy Procedia*, 2012 International Conference on Future Energy, Environment, and Materials, 16 (January):758–62. doi:10.1016/j.egypro.2012.01.122.

[122] Sólimo, Horacio N., and Ana C. Gomez Marigliano. 1993. "Excess Properties and Vapor-Liquid Equilibrium Data for the Chloroform + Tetrahydrofuran Binary System at 30°C." *Journal of Solution Chemistry* 22 (10): 951–62. doi:10.1007/BF00646606.

[128] "The BF3 Affinity Scale." 2009. In *Lewis Basicity and Affinity Scales*, 85–109. John Wiley & Sons, Ltd. doi:10.1002/9780470681909.ch3.

[136] "Viscosity, Surface Tension, Specific Density and Molecular Weight of Selected Liquids." n.d. Accessed June 20, 2022. https://www.accudynetest.com/visc_table.html.

[138] W. Ishak, W. Hafizi, N.A. Rosli, I. Ahmad, Influence of Amorphous Cellulose on Mechanical, thermal, and Hydrolytic Degradation of Poly(Lactic Acid) Biocomposites, Sci. Rep. 10 (1) (2020) 11342, https://doi.org/10.1038/s41598-020-68274-x.